Arab Academy for Science, Technology and Maritime Transport

College of Engineering and Technology

Electrical and Control Engineering Department

A Wind Energy Conversion System based on Permanent Magnet Synchronous Generator with a Parallel Connected AC-DC Buck-boost Converter

A Thesis submitted in partial fulfillment for the Degree of
Master of Science
In
Electrical and Control Engineering

By

Eng. Noha Magdy Abdelkhalek Attia

Under Supervision of

Prof. Dr. Mostafa Ibrahim Marei

Electrical Power and Machines Department

Ain Shams University

Dr. Ibrahim Abdallah Abdelsalam

Electrical and Control Engineering Department

Arab Academy for Science, Technology and Maritime Transport

Cairo
2019

Arab Academy for Science, Technology and Maritime Transport

College of Engineering and Technology

Electrical and Control Engineering Department

A Wind Energy Conversion System based on Permanent Magnet Synchronous Generator with a Parallel Connected AC-DC Buck-boost Converter

A Thesis submitted in partial fulfillment for the Degree of
Master of Science
In
Electrical and Control Engineering

By:

Eng. Noha Magdy Abdelkhalek Attia

Under Supervision of

Prof. Dr. Mostafa Ibrahim Marei

Electrical Power and Machines Department

Ain Shams University

Dr. Ibrahim Abdallah Abdelsalam

Electrical and Control Engineering Department

Arab Academy for Science, Technology and Maritime Transport

ACKNOWLEDGMENT

First of all, I would like to express my gratitude, and appreciations to my supervisors throughout the conduct of this work. I would like to express my deepest thanks to Prof. Dr. Mostafa I. Marei, professor of electrical power and machines department, Ain Shams University for his guidance and generous help.

I would like also to express my sincere thanks to Dr. Ibrahim Abdallah, doctor of electrical and control engineering, Arab Academy for Science and Technology and Maritime Transport, for his valuable supervision and scientific help.

I would like to express my sincere gratitude to Prof. Dr. Yasser Galal professor of electrical and control engineering department, Arab Academy for Science and Technology and Maritime Transport for his real support and continuous encouragement.

My deepest thanks are to Prof. Dr. Rania El Sharkawy head of electrical and control engineering department, Arab Academy for Science and Technology and Maritime Transport.

At the last but not least, I am deeply indebted to my father, my brother, and all my family members for everything, I would like to thank them for their continuous love, unstoppable encouragement, and for always believing in me.

All my work is dedicated to my mother who passed away but will always be my inspiration.

ABSTRACT

Wind power is becoming one of the cleanest and highly economical energy sources. Due to the lack of conventional resources such as fossil fuels, renewable energy sources particularly wind energy systems are rapidly developed to compete with other energy sources. Because of the variable nature of wind, various control strategies are developed to extract the maximum power from wind turbines.

In this thesis, a variable speed Wind Energy Conversion System (WECS) using a back-to-back converter has been studied. The proposed system utilizes an open-end winding Permanent Magnet Synchronous Generator (PMSG), which is getting more recognizable in the past few years. An AC-DC buck-boost converter is introduced which is examined in the Discontinuous Conduction Mode (DCM) where the current drawn from the supply is sinusoidal with unity factor. First, the single phase AC-DC converter is designed and simulated, and then the design for three-phase converter is presented followed by the back to back converter system.

The proposed WECS consists of a three-phase PMSG connected to a three parallel single-phase AC-DC cascaded converters. The control technique is divided to two main parts. The first part is dedicated for the generator-side converter utilizing the buck-boost converter to achieve Maximum Power Point Tracking (MPPT) by regulating the speed at its optimal setting and currents of the PMSG. The second control strategy is established for the grid-side converter based Voltage Source Inverter (VSI) which is responsible for the power delivered to the grid. The generator-side converter and the grid-side inverter are connected through a capacitor DC link.

Moreover, a Low Voltage Ride-Through (LVRT) strategy is integrated with the proposed scheme. Grid codes are established to provide reliability and sustainability of the electrical system. For grid connected WECS, the LVRT capability is one of the most essential requirements for the WECS to remain connected to the grid during faults. PSCAD/EMTDC simulation results are provided and discussed for the proposed converter and WECS under different operating conditions.

TABLE OF CONTENTS

1 INTRODUCTION 1

1.1 RENEWABLE ENERGY 1

1.2 WIND ENERGY 1

1.2.1 Vertical-Axis Wind Turbines 2

1.2.2 Horizontal-Axis Wind Turbines 3

1.3 WIND ENERGY CONVERSION SYSETEM 3

1.3.1 Fixed Speed Wind Turbine 3

1.3.2 Variable Speed Wind Turbine 4

1.3.2.1 DFIG Based WECS 6

1.3.2.2 PMSG Based WECS 6

1.4 GRID CODE REQUIREMENTS 8

1.4.1 General Grid Code Requirements 8

1.4.1.1 Grid Frequency Range 9

1.4.1.2 Grid Voltage Range 8

1.4.1.3 Grid Voltage Wave Form 8

1.4.2 Grid Code Requirements for Wind Turbines 9

1.4.2.1 LVRT 10

1.4.2.2 Reactive Power Control 11

1.5 THESIS METHODOLOGY 11

1.6 THESIS OUTLINE 12

2 AC-DC CONVERTERS 13

2.1 LITERATURE 13

2.2 AC-DC CONVERTERS TYPES 15

2.2.1 Cascaded Non-Inverting Buck-Boost Converter *15*

2.3 PROPOSED AC-DC CONVERTER 18

2.3.1 Simulation Results of the Proposed Buck-Boost Converter *19*

2.4 PROPOSED THREE PHASE AC-DC BUCK-BOOST CONVERTER 22

2.4.1 Simulation Results of the Proposed Buck-Boost Converter *23*

2.5 THE THREE PHASE BTB CONVERTER BASED ON BUCK-BOOST CONVERTER ... 26

2.5.1 Grid Connected BTB Three Phase Buck-Boost Converter *29*

3 MODELLING OF THE PMSG BASED WECS 34

3.1 WIND TURBINE MODEL 34

3.1.1 Wind Turbine Chtactaristic *35*

3.2 PMSG 37

3.2.1 Three Phase PMSG Model *37*

4 SIMULATION RESULTS OF THE WECS 40

4.1 MODEL DISCRIPTION 40

4.2 BUCK-BOOST CONVERTER DESIGN 41

4.2.1 MPPT Algorithm *41*

4.3 GRID SIDE VSI 42

4.4 LVRT TECHNIQUE 44

4.5 SIMULATION RESULTS 44

4.5.1 Normal Operating condition *45*

4.5.2 Operation Under Grid Fault *49*

5 CONCLUSION 53

LIST OF TABLES

Table 2-1: Simulation parameters for the single phase buck-boost converter.....19

Table 4-1: Wind turbine and PMSG parameters.....45

LIST OF FIGURES

Figure 1-1: Development of wind power generation for the past ten years. 2

Figure 1-2: HWAT and VWAT [6]. 3

Figure 1-3: WECS based SGIG for fixed speed operation. 4

Figure 1-4: WECS based WRIG for variable speed operation. 5

Figure 1-5: WECS based SGIG for variable speed operation. 5

Figure 1-6: WECS based DFIG. 6

Figure 1-7: WECS based PMSG using BTB converters. 7

Figure 1-8: WECS based PMSG using boost converter. 7

Figure 1-9: WECS based PMSG using NPC converters. 8

Figure 1-10:LVRT Characteristic for Irish Grid Code [23]. 10

Figure 1-11: LVRT Characteristic of different countries [24]. 10

Figure 2-1: Non-inverting 2-switch buck-boost converter. 16

Figure 2-2: On mode of the proposed buck boost converter. 16

Figure 2-3: Off mode for the proposed buck boost converter. 17

Figure 2-4: AC-DC buck-boost converter. 18

Figure 2-5: Proposed single phase converter. 20

Figure 2-6: Control loop for the single phase converter. 20

Figure 2-7: (a) DC output load voltage of the single phase converter and (b) Modulation Index,m. 20

Figure 2-8: (a) DC Inductor current of the single phase buck-boost and (b) Zoom in from (a). 21

Figure 2-9: Single phase AC supply voltage and current. 21

Figure 2-10: Three phase proposed buck-boost converter. 22

Figure 2-11: Proposed three phase converter. 23

Figure 2-12: Control loop for the three phase converter. 24

Figure 2-13: (a) DC output load voltage of the three phase converter, (b) Modulation index, m. 25

Figure 2-14: Inductor currents of the three phase buck-boost converter. 25

Figure 2-15: Three phase AC supply voltage and current. 25

Figure 2-16: Three phase BTB converter feeding and islanded load.....26

Figure 2-17: Control loop for the islanded three phase converter.....26

Figure 2-18: Control loop for the three phase inverter.....27

Figure 2-19: (a) Peak load voltage, (b) Input DC current for the inverter, and (c) modulation index m`. 28

Figure 2-20: AC load voltage and current.....29

Figure 2-21: Three phase BTB grid connected converter. 29

Figure 2-22: PLL for the grid voltage and current. 30

Figure 2-23: PWM technique for the three phase inverter. 30

Figure 2-24: Gating signals for the three phase inverter. 31

Figure 2-25: Three phase grid Voltage and Current. 31

Figure 2-26: (a) Grid active power, (b) modulation index m′. 32

Figure 2-27: (a) Grid Reactive Power, (b) Phase angle. 33

Figure 3-1: Total area swept by the blades [43]. 34

Figure 3-2: The power coefficient vs. tip speed ratio at different pitch angle. 36

Figure 3-3: Wind turbine active power at different wind speed. 36

Figure 3-4:Three phase and rotating refrence frame [46]. 37

Figure 4-1: Proposed WECS diagram. 40

Figure 4-2: Proposed WECS schematic diagram using EMTDC/PSCAD. 41

Figure 4-3: Proposed control loop of the buck-boost converter. 42

Figure 4-4: VSI control loops. 43

Figure 4-5: Hysteresis current control loops. 43

Figure 4-6: Generator speed and the optimal speed. 46

Figure 4-7: Grid active power and reactive power. 46

Figure 4-8: Generator peak current and the reference current. 47

Figure 4-9: Three phase generator current. 47

Figure 4-10: (a) Inductor current of the buck-boost and (b) Zoom in from (a). 48

Figure 4-11: DC link capacitor voltage. 48

Figure 4-12: Grid voltage and current. 49

Figure 4-13: LVRT capability (a) Active powers, (b) DC link capacitor voltage, (c) Generator speed..... 50

Figure 4-14: (a) the reference direct current , (b) the reference quadrature current. . 51

Figure 4-15: Grid voltage and current during fault. 52

Figure 4-16: Three phase generator current during fault. 52

LIST OF ABBREVIATIONS

GWEC	Global Wind Energy Council
WECS	Wind Energy Conversion System
VAWT	Vertical-Axis Wind Turbine
HAWT	Horizontal-Axis Wind Turbine
SCIG	Squirrel Cage Induction Generator
DFIG	Doubly-Fed Induction Generator
PMSG	Permanent Magnet Synchronous Generator
BTB	Back To Back
WRIG	Wound Rotor Induction Generator
VSC	Voltage Source Converter
VSI	Voltage Source Inverter
RSC	Rotor Side Converter
GSC	Grid Side Converter
WRSG	Wound Rotor Synchronous Generator
VSR	Voltage Source Rectifier
TSO	Transmission System Operator
LVRT	Low Voltage Ride Through
PCC	Point of Common Coupling
HVAC	High Voltage AC
HVDC	High Voltage DC

STATCOM	Static Synchronous Compensator
SVC	Static Var Synchronous
SDBR	Series Dynamic Breaking Resistor
DVR	Dynamic Voltage Restorers
SSTS	Solid State Transfer Switch
BC	Braking Chopper
ESSs	Energy Storage Systems
DCM	Discontinuous Conduction Mode
MPPT	Maximum Power Point Tracking
VSI	Voltage Source Inverter
PV	Photovoltaic
PWM	Pulse Width Modulation
HEV	Hybrid Electric Vehicle
PI	Proportional Integral
SEPIC	Single Ended Primary Inductor Converter
CSC	Current Source Converter
CCM	Continuous Conduction Mode
PLL	Phase Locked Loop
THD	Total Harmonic Distortion

LIST OF SYMBOLS

v_{dc}	The Input DC Voltage
L_{dc}	The DC Link Inductor
i_L	The Inductor Current
i_c	The Capacitor Current
v_{load}	The Converter's Output Voltage
D	The Duty Cycle
T_S	The Switching Period
m	The Amount of Air Flow
ϑ	The Wind Speed
A	The Air Swept Area
r	The Radius of the Swept Air
ρ	The Air Density
$Pwind$	The Wind Power
Cp	Power Coefficient
λ	Tip Speed Ratio
β	Blade Pitch Angle
ω	Rotor Tip Angular Speed
$Pmech$	Turbine Mechanical Power
T	Mechanical Torque of the Turbine
v_{abc}	Three Phase Stator Voltage in abc Frame

v_d	Direct Stator Voltage Component
v_q	Quadrature Stator Voltage Component
θ	Angle between Phase a and d-axis
L_{abc}	Three Phase Inductance in abc Frame
L_{aa},$L_{bb,}L_{cc}$	Stator Self-Inductance in abc Frame
$L_{ab} = L_{ba}$	Stator Mutual Inductance between Phase a and b
$L_{bc} = L_{cb}$	Stator Mutual Inductance between Phase b and c
$L_{ca} = L_{ac}$	Stator Mutual Inductance between Phase c and a
L_s	Self-Inductance Value
L_m	Mutual Inductance Value
M_s	Mutual Inductance Average value
i_{abc}	Three Phase Stator Current in abc Frame
R_s	Stator Resistance
p	Operator of Differentiation
Ψ_{abc}	Three Phase Stator Flux in abc Frame
Ψ_{fs}	Flux Linkage of the Permanent Magnet
Ψ_f	The Amplitude of the Flux Linkage by the Permanent Magnet
i_d	Direct Stator Current Component
i_q	Quadrature Stator Current Component
Ψ_d	The d-axis Flux Linkage
Ψ_q	The q-axis Flux Linkage

ω_e	The Electrical Generator Angular Speed
L_d	The d-axis Stator Inductance
L_q	The q-axis Stator Inductance
T_e	The Electromagnetic Torque
T_l	The Load Torque
ω_r	The Rotor Mechanical Angular Speed
J	The Equivalent Moment of Inertia
L_{dc}	Dc Inductor
V_{cap}	The Capacitor Voltage
i_{cap}	Capacitor Current Value
P_g	Grid Active Power in dqo Frame
v_{dg}	Grid Voltage Direct Component
i_{dg}	Grid Current Direct Component
v_{qg}	Grid Voltage Quadrature Component
i_{qg}	Grid Current Quadrature Component
Q_g	Grid Reactive Power in dqo Frame

Chapter One

1 INTRODUCTION

1.1 RENEWABLE ENERGY

Conventional energy sources such as fossil fuels become more disadvantageous due to its limitations and environmental impacts. As a result, renewable energy resources, such as solar, geothermal, biomass, wave, tidal, and wind energy appeared. Researchers are continuously and effortlessly developing techniques to extract the benefits of the available, clean, and sustainable resources [1].

Due to the variable nature of air and sun lights, the process of converting these sources into electrical energy is sometimes complicated and requires few stages especially if connected to the grid which can result in expensive initial cost [2].

1.2 WIND ENERGY

In the past decades and due to the limitation of conventional energy resources such as oil, coal, and natural gas; unlimited sources such as sun, wind, and water have been recognized for electrical energy production.

Wind generation attracts more attention than other clean energy sources and is perceived to have the lowest environmental impacts of all energy sources, leading today to more than 90 countries around the world with commercial wind generations, 9 of them with more than 10,000 MW, and 30 with more than 1,000 MW across Europe, Asia, North America, Latin America and Africa. The total installations in 2017 reached 52.492 GW, with China installing 19.7 GW; bringing the global total to 539.123 GW. The total cumulative installations are expected to reach 840 GW by the end of 2022, according to the global wind energy council (GWEC) [3].

Figure 1-1 shows the annual verses the cumulative wind power capacity over the past decade [4].

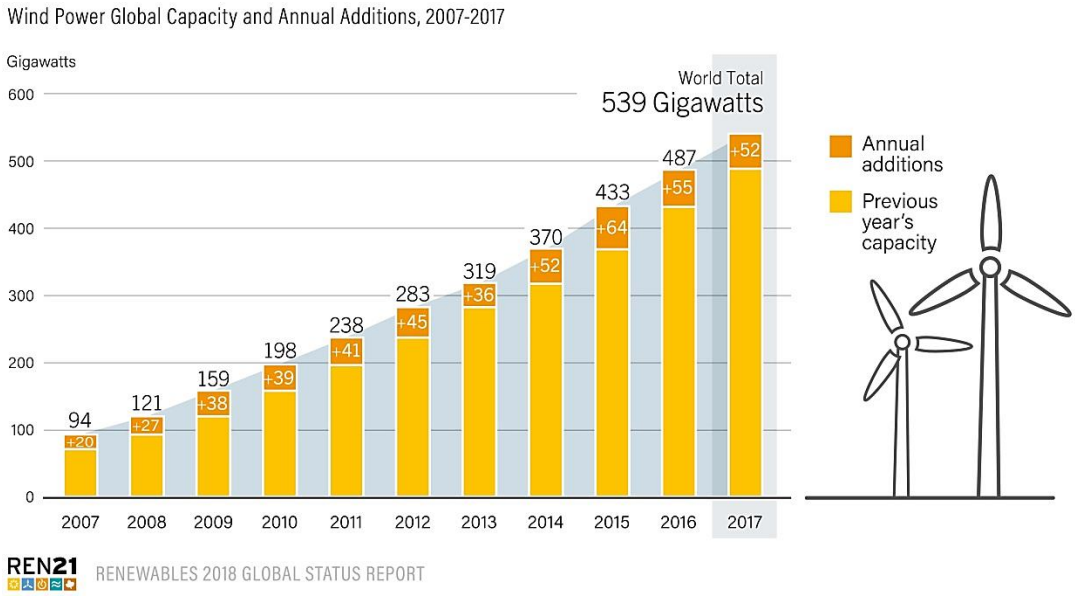

Figure 1-1: Development of wind power generation for the past ten years.

In 1980, the first ever wind farm started generating electrical power, at Crotched Mountain in Southwest New Hampshire, USA. Germany, Denmark, and Spain followed the USA. In the 1990's the market started to include Italy, the Netherlands, the UK and Sweden, then China, Japan, Canada and Australia. At the end of the 2000s and the beginning of the new decade, Brazil, Mexico and South Africa, as well as Egypt, Morocco, Chile joined the wind market.

Wind is resulted from the sun light variations, and can be transformed into kinetic energy which can then be converted into mechanical energy using wind turbines. Through the years, wind energy conversion systems (WECS) are been developed to extract the most energy captured by the blades, where the blades are linked with a turbine which is connected to the generator shaft through a gear box where all are mounted on a tower.

Wind turbines are fast and easy in installation and can either be vertical-axis (VAWT) or horizontal-axis (HAWT) [5].

1.2.1 Vertical-Axis Wind Turbines

In vertical wind turbines the rotation axis is perpendicular to the ground, where the generator and the gearbox are found at the base of the tower. It can operate at low wind speed where it is independent on the wind direction. The advantages of the VAWT is

that the cost of installation is not expensive compared to the HAWT and require less maintenance. On other hand, it is not as efficient as the HAWT; therefore, it is not commonly used in wind farms.

1.2.2 Horizontal-Axis Wind Turbines

Unlike VAWT, the rotation axis is parallel to the ground and the generator and the gear box are found at the top of the tower, where they face the wind direction. HAWT mainly consists of two or three blades, and the height of the tower is considered to be high in order to capture the wind without any obstacles, so they are more efficient but the installation cost is expensive. Figure 1-2 shows the difference between VAWT and HAWT.

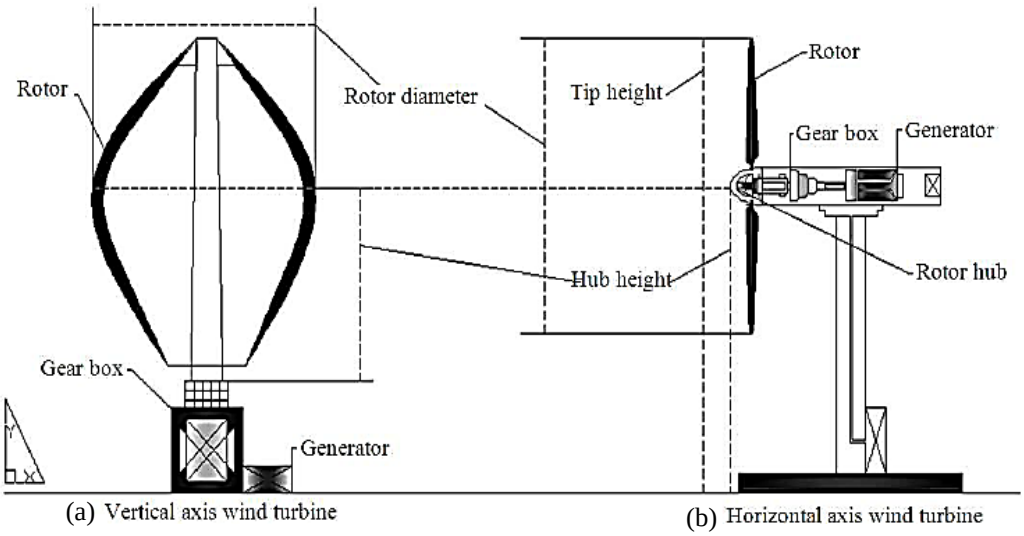

Figure 1-2: HWAT and VWAT [6].

1.3 WIND ENERGY CONVERSION SYSETEM

The wind energy conversion system (WECS) depends mainly on the wind turbine driving a generator and a control topology to extract the maximum electrical power generated while providing high reliability and less expenses. WECS can be classified to fixed-speed and variable-speed drive train [7].

1.3.1 Fixed Speed Wind Turbine

The fixed speed WECS mainly consists of a squirrel cage induction generator (SCIG) which is known for its constant speed operations and can transfer the output

generated power directly to the grid as shown in Figure 1-3. This configuration uses a capacitor bank for reactive power compensation, as the SCIG draws reactive power from the grid. The system needs a soft starter consisting of thyristors and contactors switches in order to limit the inrush stator current and to connect the generator to the grid gradually. At low wind speeds, an 8 poles generator can be used, while at medium wind speed, 4 or 6 poles SCIG are used.

This kind of operation is known for its simplicity compared to the variable speed operation which is more expensive but more efficient. The fixed speed operation transfers all the variations in the wind speed to the grid which can lead to high voltage fluctuations. Furthermore, it cannot track the speed of the wind to extract the optimum power [8].

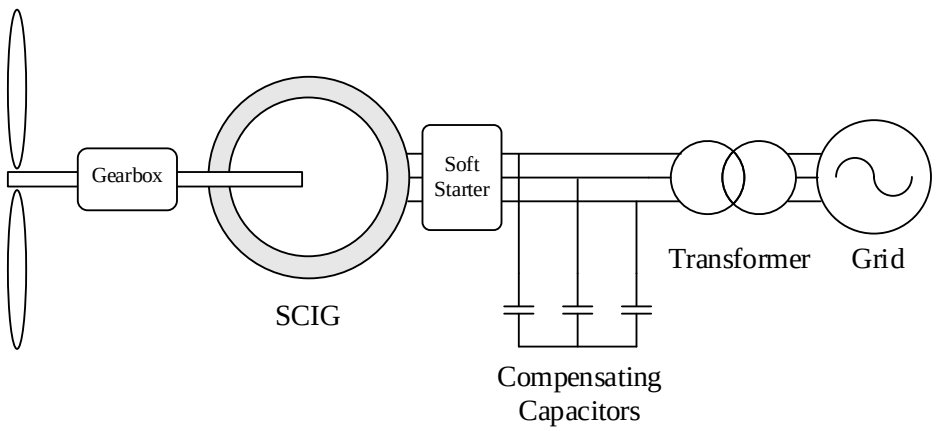

Figure 1-3: WECS based SCIG for fixed speed operation.

1.3.2 Variable Speed Wind Turbine

Variable speed wind turbines are complicated comparing to the fixed speed wind turbines because of the usage of power electronics converters, where the generator speed can be controlled to extract the maximum power regardless the variations in the wind speed.

Doubly-Fed Induction Generator (DFIG) with partial rated converter connected between the grid and rotor windings, and Permanent Magnet Synchronous Generator (PMSG) with fully rated back-to-back converter (BTB) are commonly used electrical machines in variable speed WECS.

Previously the wound rotor induction generator (WRIG) was used as in Figure 1-4, but the configuration requires an additional resistor controlled by a dc-dc chopper, connected to the rotor where it controls the energy which is dissipated in the resistor. This configuration is considered cheap but has higher rotor losses [9].

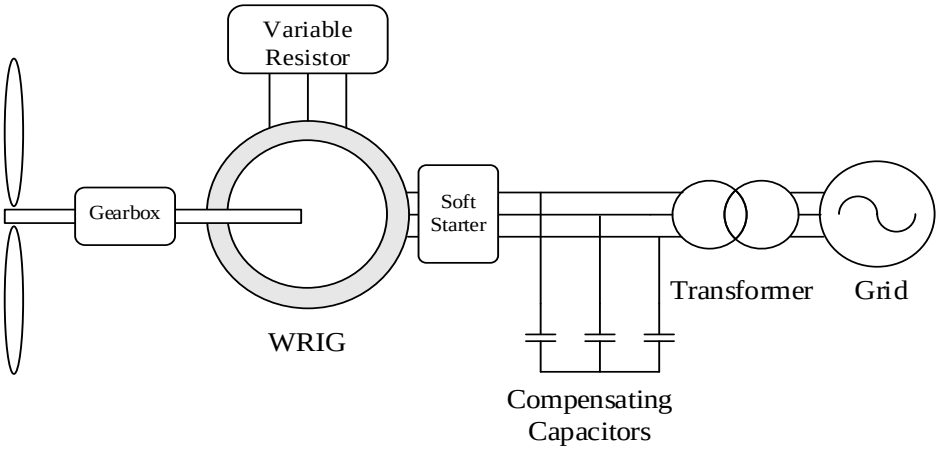

Figure 1-4: WECS based WRIG for variable speed operation.

Figure 1-5 shows a SCIG with BTB consisting of voltage source converter (VSC) and voltage source inverter (VSI) which can be used in variable speed operations; however, the converters are oversized and cost much [10].

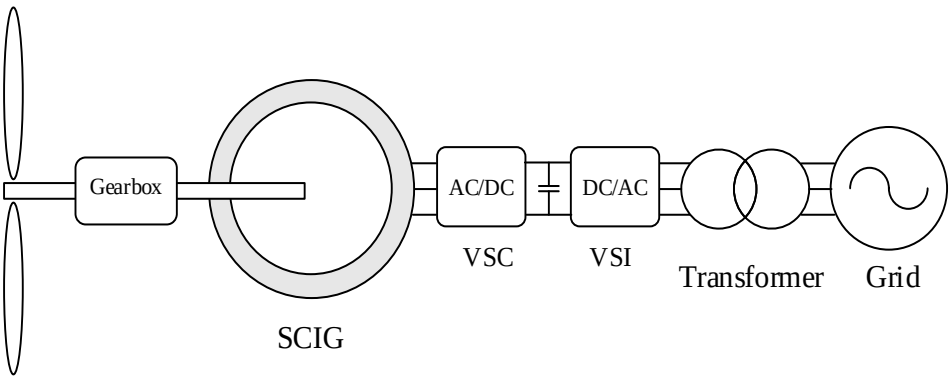

Figure 1-5: WECS based SCIG for variable speed operation.

The variable speed operations depends mainly on power converters which help capturing the most out of the wind energy developed by the turbine, but the usage of such converters sometimes add to the expense of the system making it more complex, although it improves the power quality and reduces the mechanical stress.

1.3.2.1 DFIG Based WECS

The DFIG- wound rotor- is widely used in WECS for a long time where its stator is connected directly to the grid and its rotor is also connected to the grid via partial rated power converter consisting of a rotor side converter (RSC) to control the machine speed, and a grid side converter (GSC) to control the DC-link voltage or vice versa (Figure 1-6). The reactive power is controlled by both RSC and GSC. The slip power is delivered to the grid by the BTB converter [11].

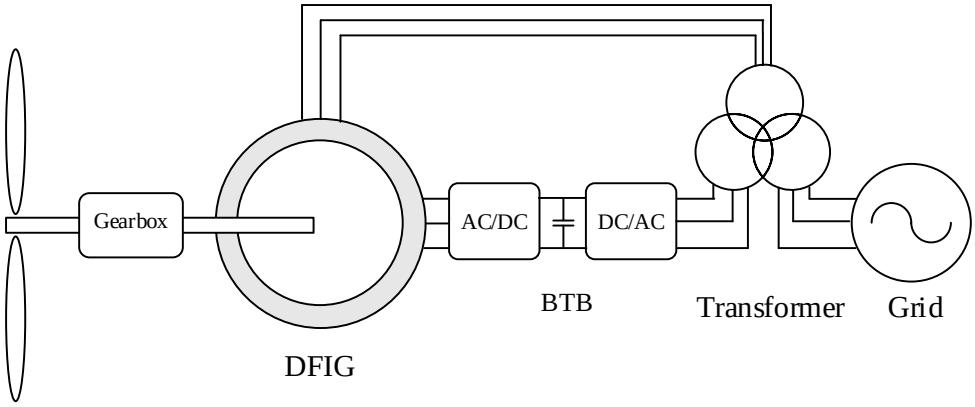

Figure 1-6: WECS based DFIG.

Another configuration can be obtained using AC-AC converter or hybrid voltage source/ current source inverters [12].

The main advantage is that only 30% of the generator rated power can get through the converters. The main drawbacks are partial speed operation and the presence of slip rings in induction generators requires frequent change which leads to regular maintenance and may lead to machine failure. Induction generators are preferred for low power application [13].

1.3.2.2 PMSG Based WECS

Synchronous generators based WECS are known for its wide speed-range control, having higher efficiency with nearly unity power factor. When connected to a wind turbine, the rotor speed depends on the wind speed. They are said to be more stable than the induction generators [14].

Wound rotor synchronous generator (WRSG) was introduced as a variable speed WECS generator, but the presence of DC brushes for excitation requires frequent change [13]. The configuration can be achieved using BTB converters, consisting of a RSC and a GSC.

PMSG was then an attractive solution for the WECS with large scale wind turbines; above 1 MW, with its main advantages of the absence of brushes, slip rings, and rotor windings which are replaced by the permanent magnet; all lead to decreasing the generator weight and increases the reliability

The configuration for low voltage wind turbines can be achieved by a full capacity BTB where the RSC can be built using diodes as voltage source rectifiers (VSR), and a VSI as a GSC as shown in Figure 1-7 [15].

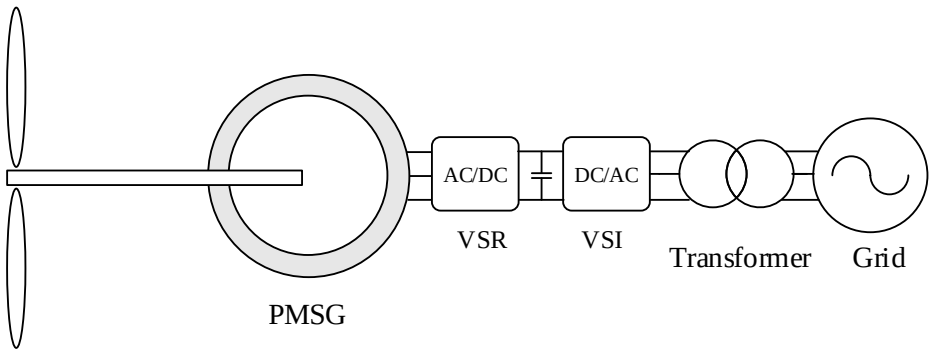

Figure 1-7: WECS based PMSG using BTB converters.

Instead of using only diode rectifiers, a DC-DC chopper is added to the RSC in order to boost the voltage and to control the maximum power of the wind turbine (Figure 1-8) [16].

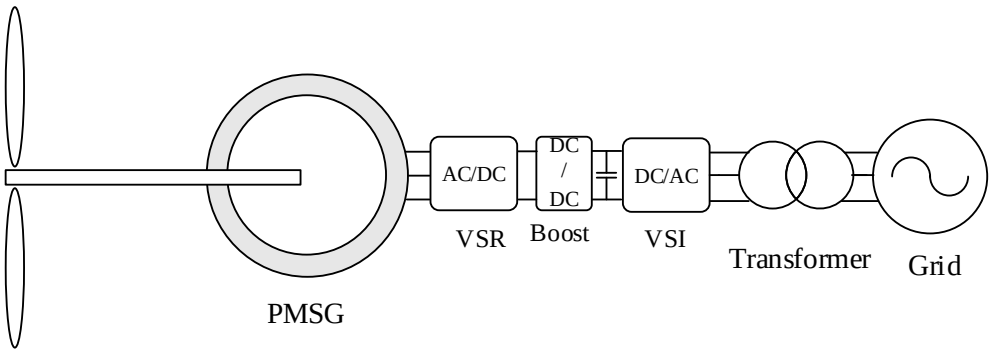

Figure 1-8: WECS based PMSG using boost converter.

Another configuration is illustrated in Figure 1-9 for medium voltage wind turbines using neutral point clamped converters (NPC) [17].

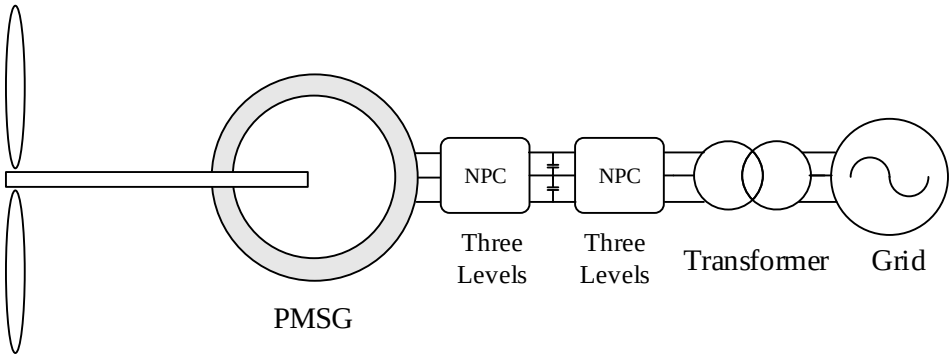

Figure 1-9: WECS based PMSG using NPC converters.

PMSG can be considered a direct-drive wind turbine where the shaft of the rotor can be connected directly to the wind turbine without gearbox, and do not requires any external current excitation, which make it suitable for low speed operations up to 30 rpm but the operation requires a large size PMSG with high poles number.

For medium speed operation up to 400 rpm, medium size PMSG with a single stage or two stages gearbox is used for wind turbines between 1MW to 10 MW, while high speed operation requires a three stage gearbox and a small size PMSG [18].

1.4 GRID CODE REQUIREMENTS

1.4.1 General Grid Code Requirements

Grid codes are the rules laid by the transmission system operator (TSO) for the generating power plant in order to be able to connect to the network and operate as per the standards. These codes are considered the guide lines to ensure the stability and the consistency of the grid for both the users and consumers. One of the most important classifications for the grid code is the connecting code, which specifies the operational, design and technical requirements, such as the voltage fluctuations and wave form quality, and the frequency variations where all the different components connected together must be synchronized to avoid disconnection of the plant [19].

Every country has its own grid code which depends on the nature of the grid, the load, and the type of the electrical power stations supplying the grid [20].

1.4.1.1 Grid Frequency Range

Due to the variation of the WECS component, any imbalance in frequency will lead to loss of the link between the connected components. Therefore, the frequency must be maintained within the prescribed limits. The Frequency of the National Electricity Transmission System shall be nominally 50Hz and shall be controlled within the limits of 49.5 - 50.5Hz [21].

1.4.1.2 Grid Voltage Range

Similar to the frequency, the voltage variation must be kept within permissible range. Where at lower voltage level, the voltage may vary at larger scale than at higher voltage levels[22].

1.4.1.3 Grid Voltage Wave Form

Due to the nonlinearity of the power plant components, it leads to wave form distortion and voltage fluctuations. Where the power plant must be able to withstand the following distortions of the voltage waveform [23] :

i. **Harmonics:** The harmonic distortion as a result of the switching of the different power electronics devices attached to the system must be within certain limits according to each country [24].

ii. **Phase Unbalance:** Phase unbalance occurs due to loading on the transmission system between the operator and the users. Therefore, certain regulations must be followed by the power plants and the users.

1.4.2 Grid Code Requirements for Wind Turbines

As the renewable power plants becoming an essential among other conventional ones, grid codes were upgraded to overcome the variable nature of the renewable energy resources.

For WECS, the most important requirements apart from the power quality are the low voltage ride through (LVRT) capability and the reactive power control, where these requirements are often specified at the point of common coupling (PCC) between the

wind farm and the network [25]. The latest grid codes demand that during severe grid disturbances, the wind farms must remain in operation and that the active power must be regain its value as before the fault levels as soon as the fault is cleared and in certain cases injecting reactive current in order to support grid voltage during disturbances [26].

1.4.2.1 LVRT

Faults may lead to voltage dip/sags, and since that the codes require that the wind farm must be connected and operating during faulty conditions, the grid code for LVRT is basically a voltage versus time characteristic stating the minimum value for the wind turbine to be connected as shown in Figure 1-3, and Figure 1-4.

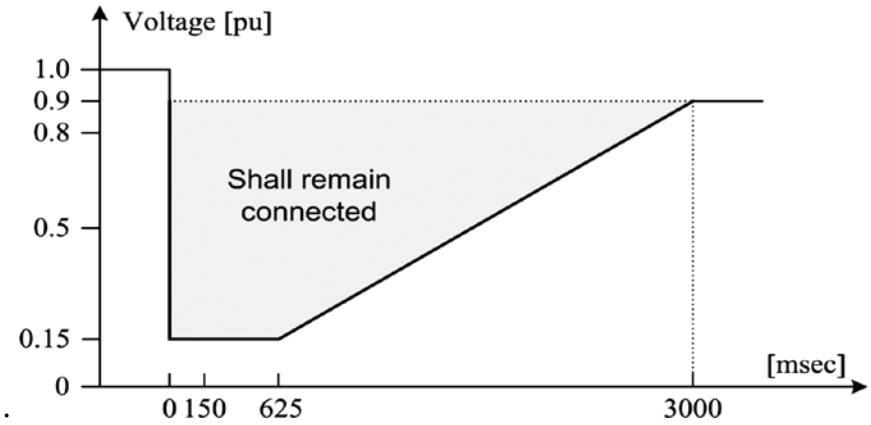

Figure 1-10:LVRT Characteristic for Irish Grid Code [27].

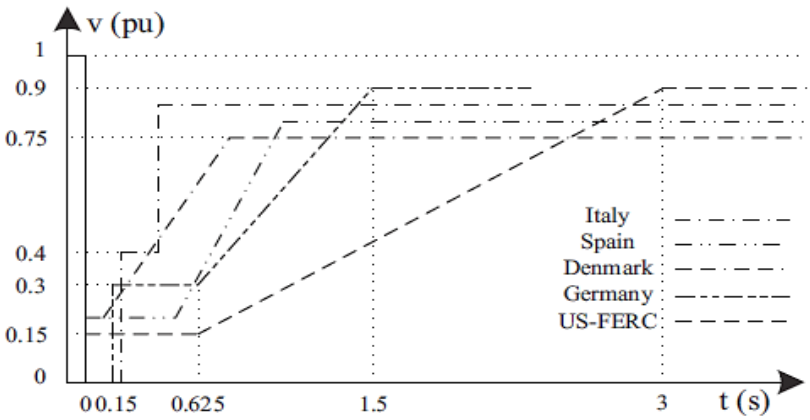

Figure 1-11: LVRT Characteristic of different countries [28].

Various methods have been developed for LVRT depending on the grid connection to the wind farm where it's either using high voltage AC (HVAC) transmission lines for large wind farms or high voltage DC (HVDC) lines for off shore wind farms.

Static synchronous compensator (STATCOM), static var compensator (SVC), and series dynamic breaking resistor (SDBR) can be used as a solution for WECS connected to HVAC [27]. Also, dynamic voltage restorers (DVR), solid state transfer switch (SSTS) have been used for power flow control [29].

In the case of DFIG based wind turbines, the stator is directly connected to the grid which results in severe transients for large grid disturbances. DVR and crowbar are used for DFIG[30].

For PMSG, LVRT can be achieved using braking chopper (BC) or active crowbar, and energy storage systems (ESSs).

1.4.2.2 Reactive Power Control

Similar to the conventional power plants, it is mandatory to maintain the reactive power levels, especially for large wind turbines. It is important for the connected wind turbine to maintain the power factor within the range of 0.95 lagging to 0.95 leading. The reactive power control assists in sustaining the voltage stability, this can be successfully achieved in variable speed WECS where the power electronics controllers, can be easily controlled [31].

1.5 THESIS METHODOLOGY

The objective of this thesis is to propose an ac-dc buck-boost converter which has a reduced voltage stress and current stress per power electronic switch for a PMSG based WECS. The proposed AC-DC buck-boost converter is operated under discontinuous conduction mode (DCM) and fulfils the grid code requirements during normal and faulty conditions where the system performance was examined during LVRT. The WECS topology consists of an open winding three phase PMSG connected to the grid using a BTB converter, where the generator-side converter consists of three uncontrolled rectifiers cascaded with the proposed buck-boast converter to achieve the maximum power point tracking (MPPT) and control the PMSG current. The GSC

consists of a voltage source inverter (VSI) which controls the active and the reactive power fed to the grid. The generator-side converter and the GSC are connected through a capacitor dc link.

1.6 THESIS OUTLINE

In chapter 2, the literature review and the common types of ac-dc converters are discussed. Moreover, the proposed cascaded non-inverting buck-boost converter is introduced with simulation results under several cases. Chapter 3 presents the dynamic model for the wind turbine and the three phase PMSG model in the dqo frame. In chapter 4, the proposed WECS is examined along with the control techniques and the simulation results using PSCAD/EMTDC program. Finally, Chapter 5 presents the conclusion of the thesis.

Chapter Two

2 AC-DC CONVERTERS

2.1 LITERATURE

Two-switches, non-inverting buck-boost converter is proposed in [32] for the applications of photovoltaic (PV) system. The gate signals for the switches were produced using pulse width modulation (PWM) technique and fuzzy proportional-integral (PI) controller to compare the dynamic response for the output voltage in both cases.

In [33], four-switches non-inverting buck-boost converter was presented. It is controlled to overcome the dead zone issue which affects the performance of the converter when switching from buck mode to boost mode and vice versa. Multimode modulation technique was applied in order to enhance the operation of the DC-DC converter.

An AC-DC converter consisting of a diode rectifier and a non-inverting buck-boost converter is introduced in [34]. A PMSG is feeding the AC-DC converter so as to charge the batteries required for the hybrid electric vehicle (HEV). The converter is controlled to regulate the output DC voltage.

The three-phase series connected AC-DC buck-boost converter proposed in [35] is operating under DCM of the dc-link inductance current. The proposed ac-dc converter has a sinusoidal supply current with unity power factor over wide range of operation. In addition, the series connection reduced the voltage stress of power electronics switches. However, the operation under DCM results in a high current stress on the power electronic elements that limits the rated power of the proposed converter.

The current stress issue of the ac-dc buck-boost converter that operates under DCM was discussed in [36]. Two reduced current stress AC-DC buck-boost converters operating under DCM are proposed.

In the first topology, the converters are charged in series and discharged in parallel, while in the second topology the converters are charged in parallel and discharged in series. It has been shown that the second topology has the lowest current stress on the power electronics switches.

The WECS based PMSG presented in [37] ,consists of a diode rectifier series with a single ended primary inductor converter (SEPIC) to maintain the DC bus voltage. The control loop for the SEPIC was designed to achieve MPPT.

In [38], the control of variable speed generators, where their scheme consists of a conventional three phase AC-DC converter which is connected to grid side inverter through DC link is studied. A simple PWM technique was implemented to achieve MPPT.

A low cost WECS is presented in [39], where a PMSG is connected to the grid through a BTB converter. A 2-switches non inverting buck-boost converter was introduced to control the DC link voltage which is connected to the grid side inverter to supply the grid with the needed active power.

For the purpose of battery charging and the importance of using batteries as a storage device; the authors of [40], studied the system using a small wind turbine connected to a PMSG followed by AC-DC converter consisting of a non-inverting buck-boost converter and an uncontrolled rectifier.

To compare between direct drive PMSG of low speed and a medium speed PMSG with single stage gearbox, a simple approach was introduced in [18] for the generator side converter and the grid side inverter in order to regulate the DC link voltage and to track the MPP of operation while supplying the grid with active power and following the grid code . In [41], a three level boost converter and NPC inverter are introduced as a BTB converter for a WECS based PMSG to overcome the disadvantages of the conventional inverters.

In [42], a conversion system for wind turbine is presented to meet the grid code requirements, where a PMSG is feeding a diode rectifier cascaded with a boost converter to step up the voltage of the DC link, and then a traditional VSI is delivering

the power to the grid. The controllers for the boost converter is based on perturb and observe (P&O) technique.

2.2 AC-DC CONVERTERS TYPES

A typical AC-DC converter can be achieved using a controlled rectifier. The rectifier is built using thyristors, which can be controlled to vary the output DC voltage. In this case, the PMSG is connected to the rectifier followed by a PWM inverter, or a z-source inverter [43].

Another AC-DC converter used for WECS is the rectifier-chopper by using an uncontrolled diode rectifier cascaded with a buck, boost, or a buck-boost converter. The main advantage of using the buck-boost converter is that MPPT can be achieved by controlling the duty cycle of the converter.

Other configuration using dc-dc choppers are introduced in [44], including cuk and SEPIC.

The generator side ac-dc converter and the GSC are usually connected using a capacitor for a VSC or an inductor for a current source converter (CSC).

2.2.1 Cascaded Non-Inverting Buck-Boost Converter

The topology of the non-inverting buck-boost converter consists of a buck converter cascaded with a boost one where both are connected with a single coil to ensure that the output voltage have the same polarity as the input voltage.

The usage of such converter is not limited to the WECS, but it became a hot topic for PV, dc-batteries, and electrical vehicles [45].

Figure 2-1 shows the 2- switch topology which contains two switches two diodes. Another topology can be achieved with the use of 4 switches.

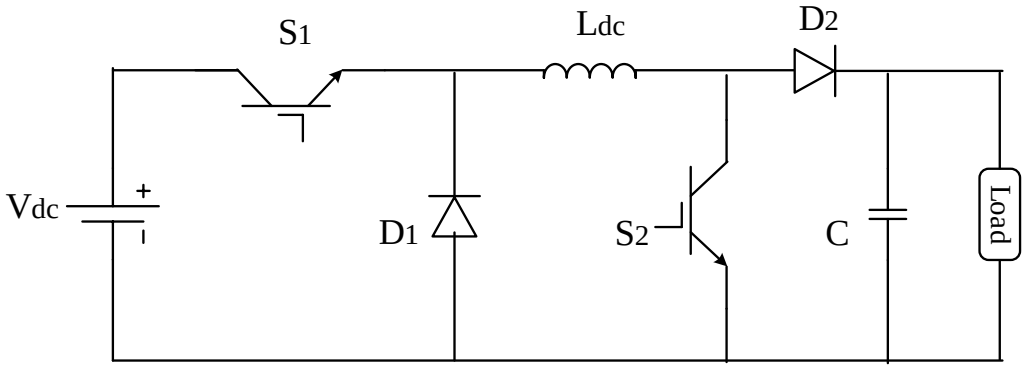

Figure 2-1: Non-inverting 2-switch buck-boost converter.

When S_1 and S_2 receive the gate signal simultaneously, both switches are on allowing the inductor to charge during the on mode. While at the off mode, the inductor will be discharging causing the capacitor to charge. If the duty cycle is less than 0.5, the converter will act as a buck, and if it is greater than 0.5, the converter will act as a boost converter for the case of continuous conduction mode (CCM).

It can also work at either buck mode when S_1 is modulated and S_2 is turned off, or boost mode when S_2 is modulated and S_1 is turned on.

- **On Mode**

When S_1 and S_2 are turned on, the energy flows from the supply and will be stored in the inductor L_{dc} , and the capacitor is supplying the load as shown in Figure 2-2.

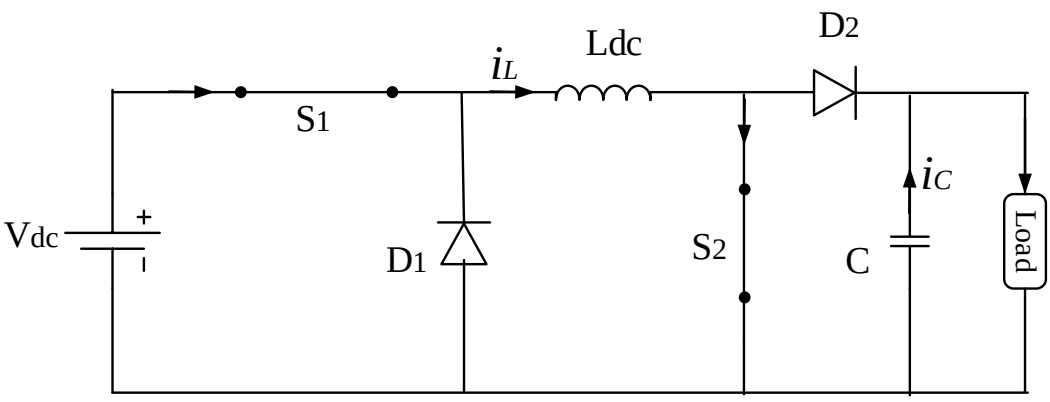

Figure 2-2: On mode of the proposed buck boost converter.

The voltage drop on the inductor is equal to the input DC voltage v_{dc} as follow,

$$v_{dc} = L_{dc}\frac{di_L}{dt} \tag{2.1}$$

$$\frac{dv_{load}}{dt} = -\frac{1}{c}i_c \tag{2.2}$$

Where L_{dc} is the DC link inductor, i_L is the inductor current, i_c is the capacitor current, and v_{load} is the converter's output voltage.

- **Off Mode**

When S_1 and S_2 are turned off, the energy of the inductor L_{dc} is transmitted to the load and charging the capacitor through the diodes D_1 and D_2 as in Figure 2-3.

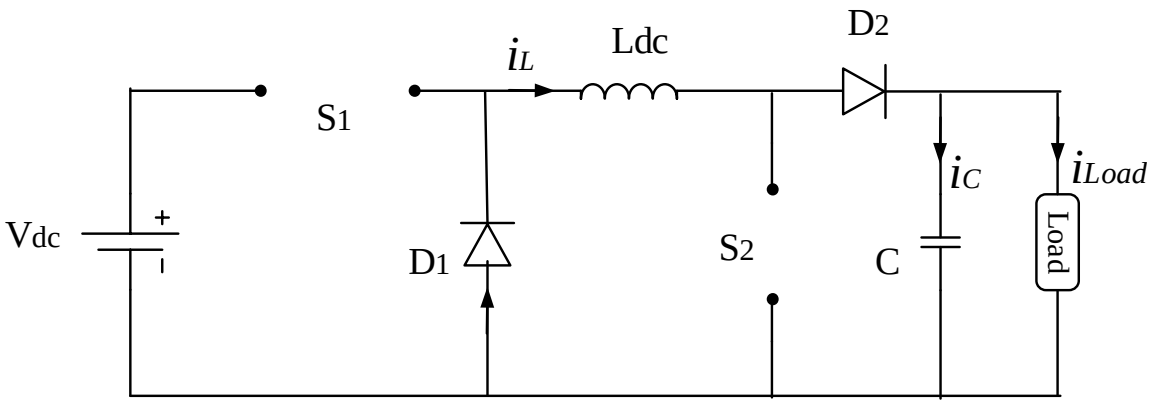

Figure 2-3: Off mode for the proposed buck boost converter.

$$v_{Load} = -L_{dc}\frac{di_L}{dt} \tag{2.3}$$

$$i_L = i_C + i_{Load} \tag{2.4}$$

The duty cycle is calculated as follow,

$$D = \frac{V_{out}}{V_{out}+V_{in}} = \frac{V_{Load}}{V_{Load}+V_{dc}} \tag{2.5}$$

The converter can operate under CCM or under DCM. During DCM, the converter is operating through three intervals, the on-mode where the dc-link inductance is charging, the off-mode where the dc-link inductance is discharging, and the zero-current mode.

2.3 PROPOSED AC-DC CONVERTER

The proposed single-phase AC-DC converter is shown in Figure 2-4, which consists of an uncontrolled bridge rectifier cascaded with a non-inverting 2-switches buck-boost converter operating under DCM. The current drawn from the supply is sinusoidal at unity power factor and the voltage stress over the switches is minimized. The voltage stress is divided on both switches and diodes.

The switching frequency for both switches is selected to be much higher than the supply frequency (usually in the range of several kHz).

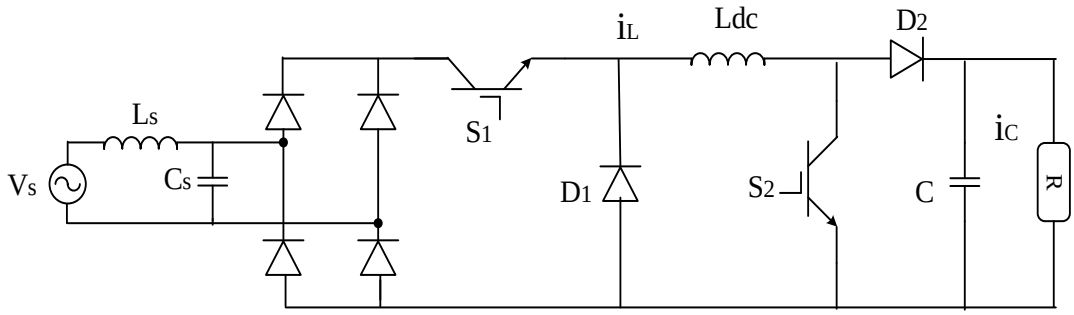

Figure 2-4: AC-DC buck-boost converter.

While operating under DCM, the converter will be working through three intervals of time as follow:

- **The first interval** where S_1 and S_2 are both on, the DC inductor L_{dc} is charging and the DC capacitor C is supplying the resistive load R with approximately constant current ($0 < t < t_{on}$).

$$v_{dc} = L_{dc}\frac{di_L(t)}{dt} \tag{2.6}$$

$$i_c(t) = -\frac{v_{load}}{R} \tag{2.7}$$

Where $t_{on} = DT_S$ and T_S is the switching period.

- **The second interval** where S_1 and S_2 are both off, the DC inductor L_{dc} is discharging through the DC capacitor and the resistive load till it is fully discharged where the energy stored in the inductor during the first interval reaches zero ($t_{on} < t < t_x$).

$$v_{load} = -L_{dc}\frac{\mathrm{di_L(t)}}{\mathrm{dt}} \tag{2.9}$$

$$i_L(t) = i_C(t) + i_{Load}(t) \tag{2.10}$$

- **The third interval** where S_1 and S_2 are still off, and the energy stored in the inductor is equal to zero. Therefore, the inductor current is also zero ($t_x < t < T_s$). From (2.10),

$$i_L(t) = i_C(t) + i_{Load}(t) = 0 \tag{2.11}$$

$$i_c(t) = -\frac{v_{load}}{R} \tag{2.12}$$

2.3.1 Simulation Results of the Proposed Buck-Boost Converter

The simulation for the proposed converter is obtained using EMTDC/PSCAD program where the parameters are presented in Table 2-1.

Table 2-1: Simulation parameters for the proposed single phase buck-boost converter.

Converter Parameters	
Supply Phase voltage (L-G), V_s	1.95 KV
DC Inductor, L_{dc}	0.001 H
DC Capacitor, C	2200 μF
AC Inductor, L_s	0.003 H
AC Capacitor, C_s	50 μF
Load Resistance, R	108 Ω
Switching frequency	2.4 kHz

Figure 2-5 shows the circuit diagram, where the PWM technique is used to obtain the gating signal for the switches. First, a PI was used to regulate the output voltage at its desired level, 6 KV, as in Figure 2-6.

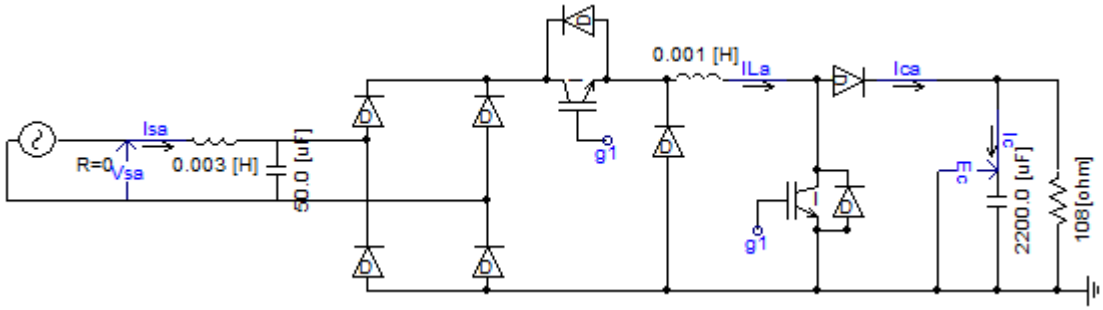

Figure 2-5: Proposed single phase converter.

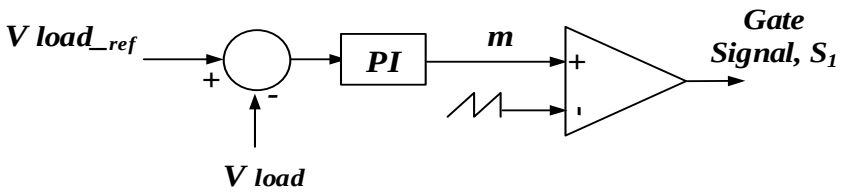

Figure 2-6: Control loop for the single phase converter.

Figure 2-7 shows the load voltage and the modulation index m in Figure 2-7(a) and Figure 2-7(b) respectively. It can be observed that the converter was able to track the controller where the voltage is maintained constant at 6 KV.

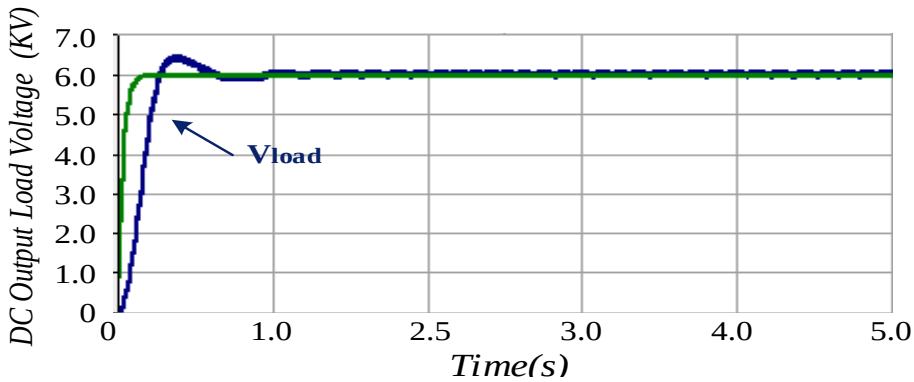

(a)

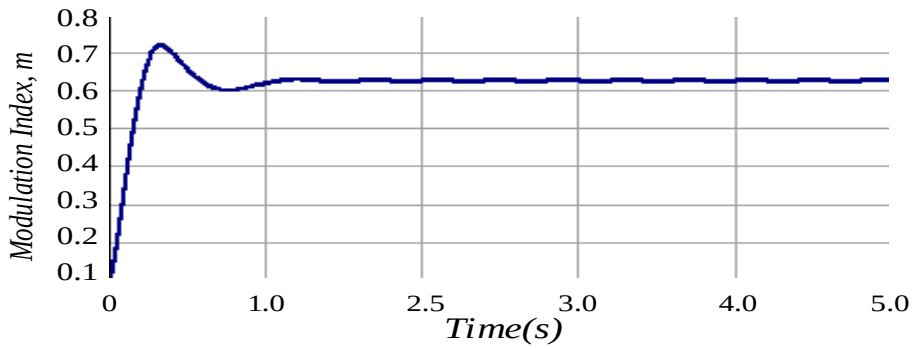

(b)

Figure 2-7: (a) DC output load voltage of the single phase converter and (b) Modulation Index,m.

In figure 2-8, the DC inductor current L_{dc}, is illustrated in Figure 2-8(a), while in Figure 2-8(b) a close-up is shown for the DCM operation.

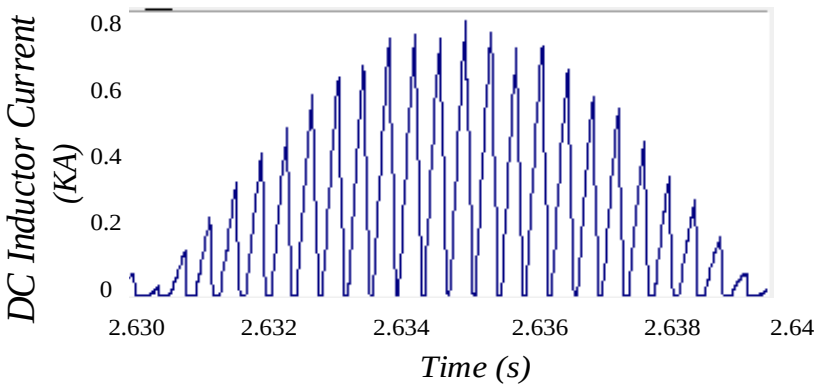

(a)

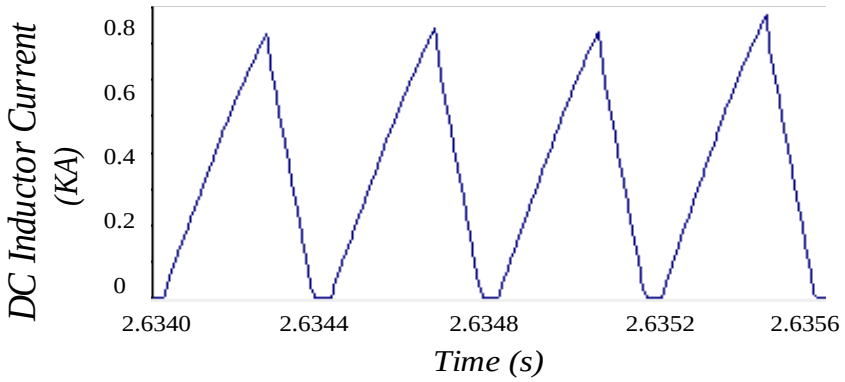

(b)

Figure 2-8: (a) DC Inductor current of the single phase buck-boost and (b) Zoom in from (a).

Finally, the AC input voltage and current for the rectifier are seen in figure 2-9, where both the supply voltage and current are sinusoidal and in phase.

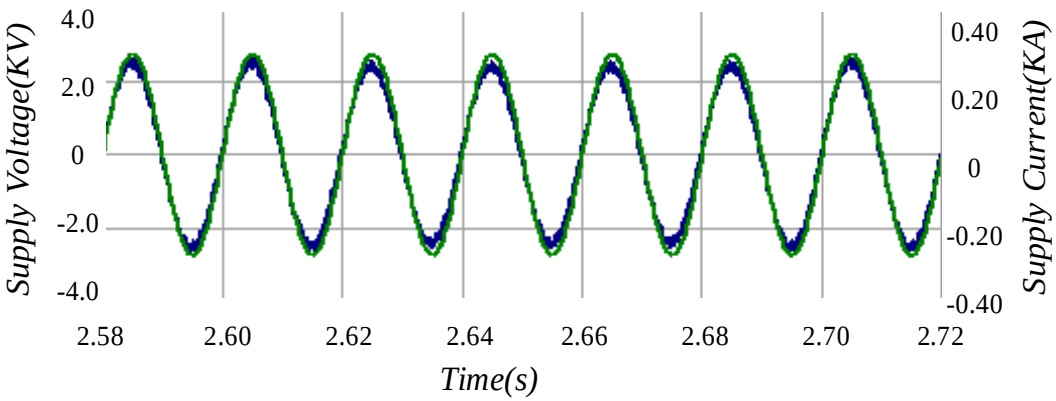

Figure 2-9: Single phase AC supply voltage and current.

2.4 PROPOSED THREE PHASE AC-DC BUCK- BOOST CONVERTER

The proposed converter consists of a three single phase AC-DC buck-boost converters operating under DCM where there output DC voltages are connected in parallel, as in figure 2-10, to the load side.

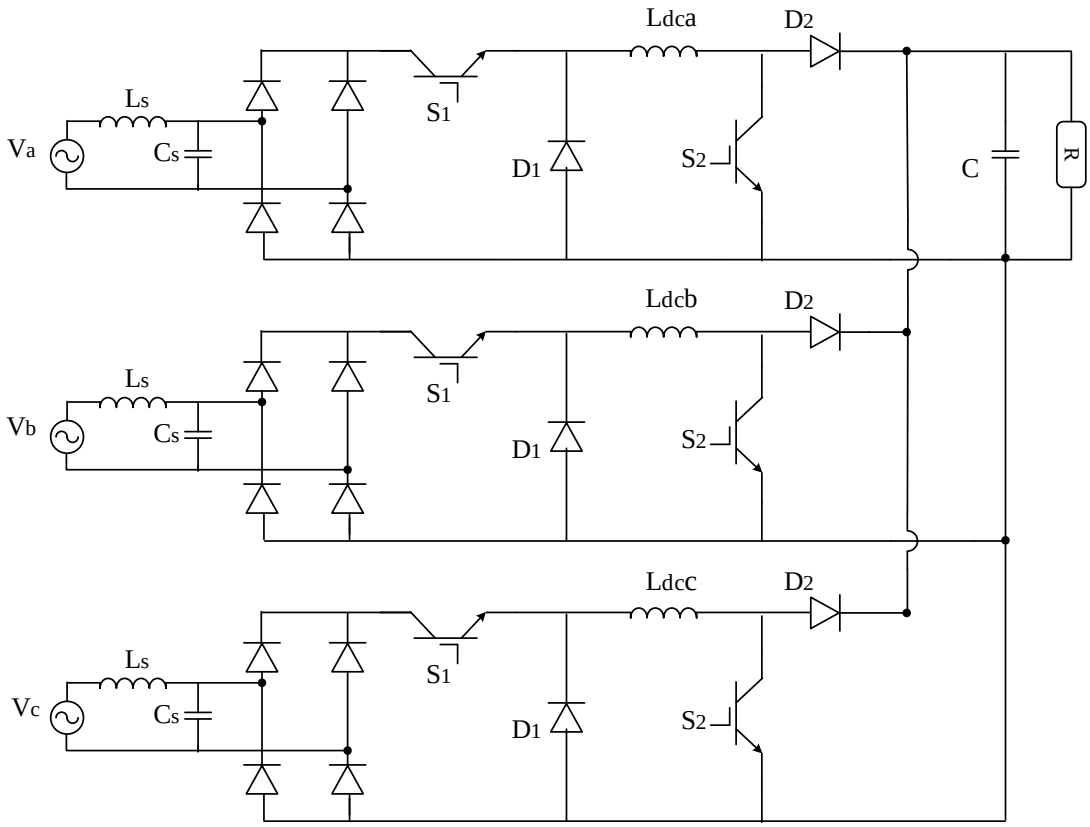

Figure 2-10: Three phase proposed buck-boost converter.

For the design of the circuit, the three AC-DC converters are identical, where $L_{dca} = L_{dcb} = L_{dcc}$.

Where the three phase supply voltage are as in (2.13):

$$v_a = v_m \sin(\theta_s) \tag{2.13}$$

$$v_b = v_m \sin\left(\theta_s - \frac{2\pi}{3}\right)$$

$$v_c = v_m \sin(\theta_s + \frac{2\pi}{3})$$

- **The first interval** ($0 < t < t_{on}$).

$$i_c(t) = -\frac{v_{load}}{R} \tag{2.14}$$

- **The second interval** ($t_{on} < t < t_x$), the DC voltage across the inductors will be expressed as follow:

$$v_{la} = -L_{dca}\frac{di_{La}(t)}{dt} \tag{2.15}$$

$$v_{lb} = -L_{dcb}\frac{di_{Lb}(t)}{dt}$$

$$v_{lc} = -L_{dcc}\frac{di_{Lc}(t)}{dt}$$

$$i_{La}(t) + i_{Lb}(t) + i_{Lc}(t) = i_C(t) + i_{Load}(t) \tag{2.16}$$

- **The third interval** ($t_x < t < T_s$).

$$i_c(t) = -\frac{v_{load}}{R} \tag{2.17}$$

2.4.1 Simulation Results of the Proposed Buck-Boost Converter

The simulation results are obtained using the same parameters as in Table 2-1, whereas the three phase load resistance is equals to 36 Ω as shown in Figure 2-11.

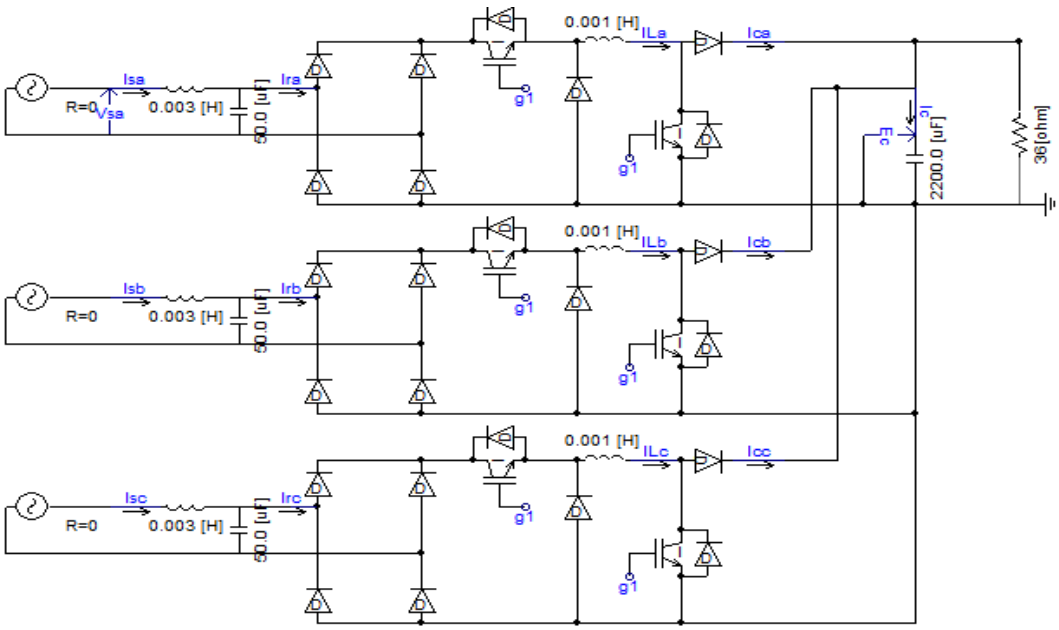

Figure 2-11: Proposed three phase converter.

The gating signals were obtained using a double control loop. In the first control loop, a PI is used to regulate the DC output voltage at its reference value. This loop generates the AC supply peak current which will then be compared to its actual value using another PI controller. The gate signal is generated using a PWM technique as shown in Figure 2-12.

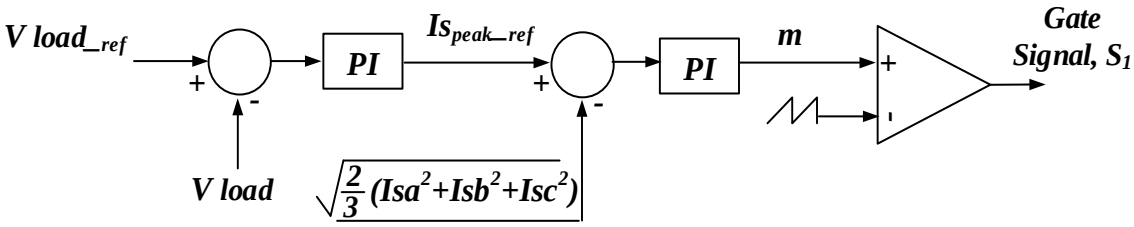

Figure 2-12: Control loop for the three phase converter.

The DC voltage and the modulation index, m are shown in Figure 2-13(a) and (b) respectively. The controller succeeded to maintain the load voltage at its reference value, also the DC inductor currents is operating at DCM as shown in Figure 2-14. In Figure 2-15, the sinusoidal supply three phase current and phase 'a' for the supply voltage are shown in phase.

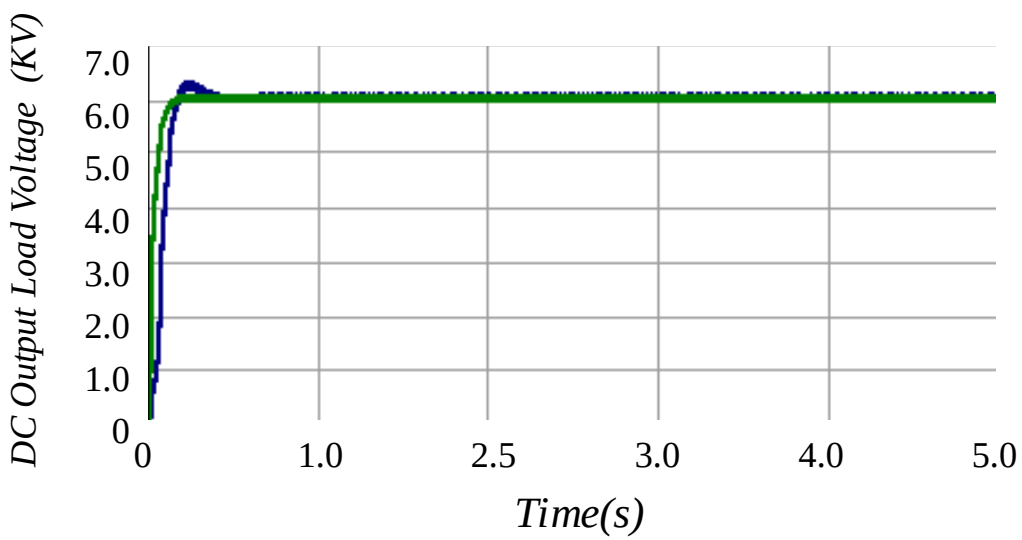

(a)

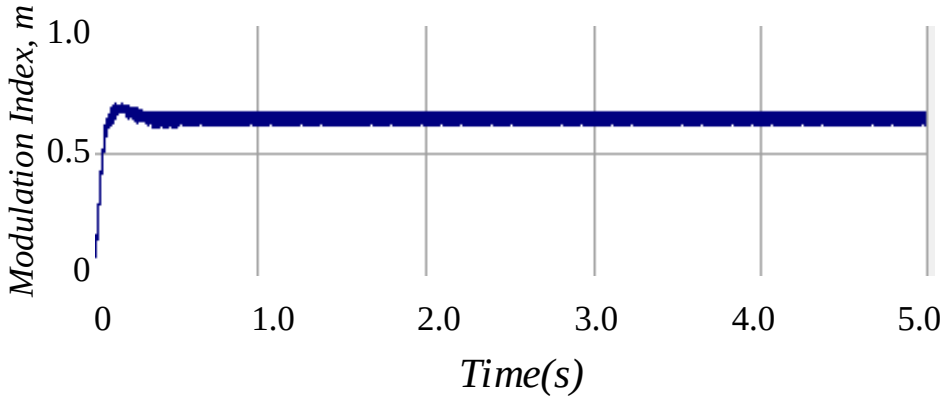

(b)

Figure 2-13: (a) DC output load voltage of the three phase converter, (b) Modulation index, m.

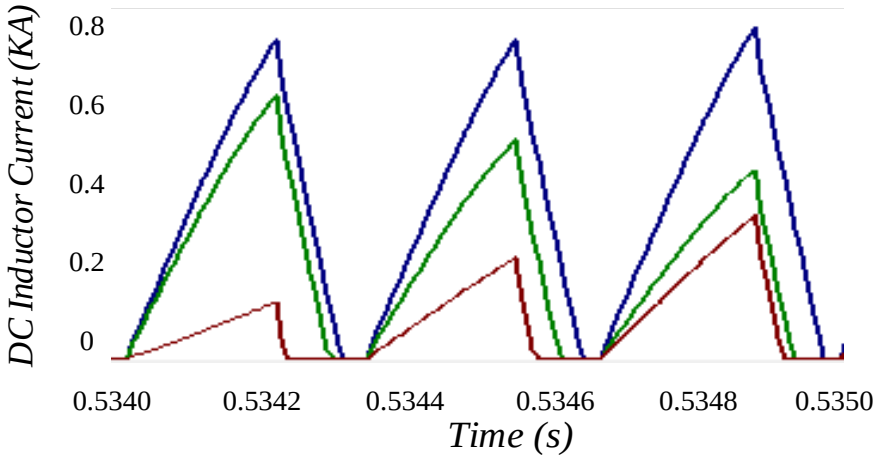

Figure 2-14: Inductor currents of the three phase buck-boost converter.

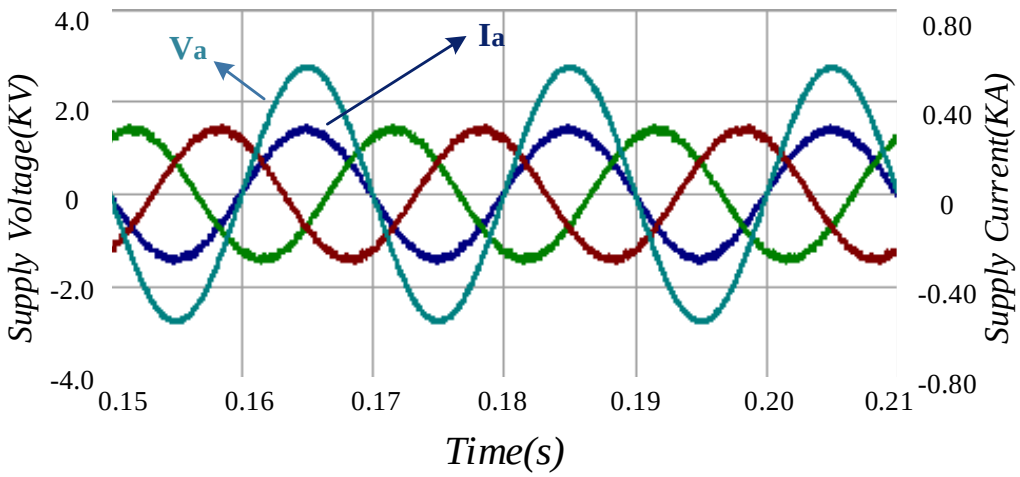

Figure 2-15: Three phase AC supply voltage and current.

2.5 THE THREE PHASE BTB CONVERTER BASED ON BUCK-BOOST CONVERTER

The AC-DC three phase buck-boost converter is connected to a three phase voltage source inverter in order to form the proposed BTB converter, shown in Figure 2-16.

The simulation was firstly done for the islanded BTB converter. The same parameters of Table 2-1 are used where the three phase load resistors are set to be equal to 20.83 Ω; however, after 3 seconds a step change would occur where the load resistance drops to half its value.

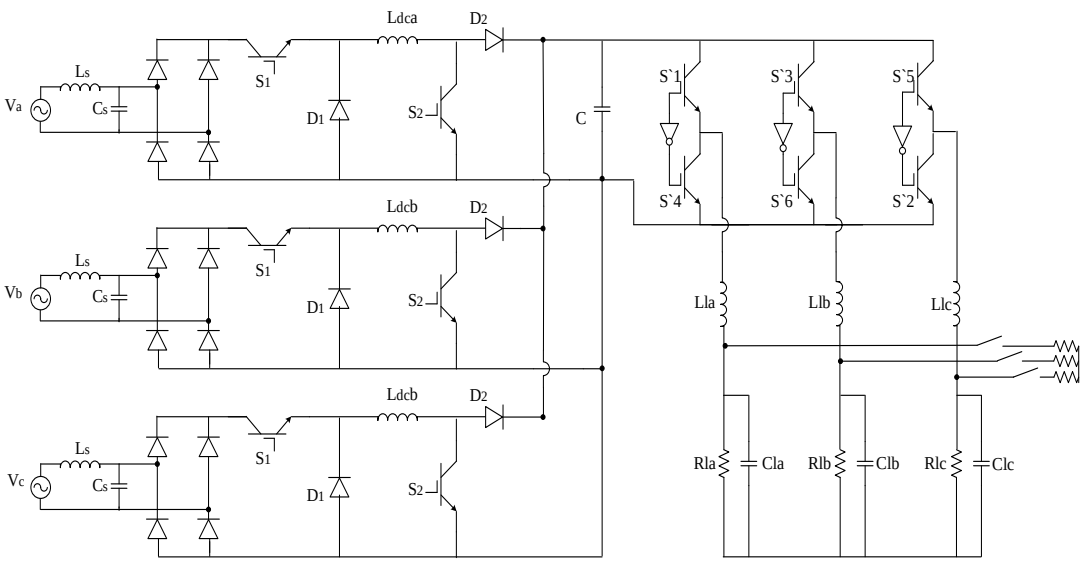

Figure 2-16: Three phase BTB converter feeding and islanded load.

The control loop for obtaining the gate signals for the buck-boost converter is shown in figure 2-17, where the DC link capacitor voltage is regulated at its reference value.

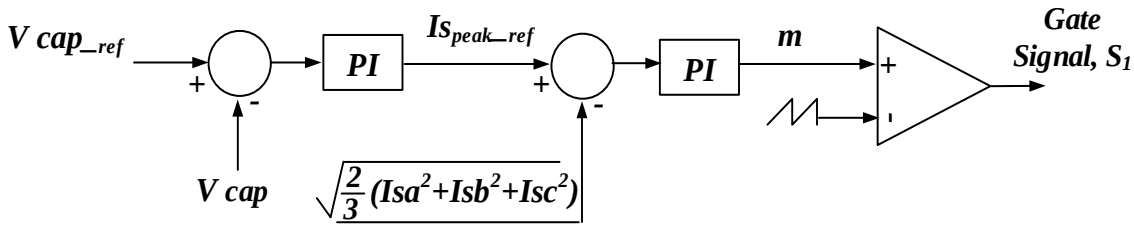

Figure 2-17: Control loop for the islanded three phase converter.

For the inverter's gating signals, a double control loop is used where a PI is used to regulate the three phase load voltage at its reference value, then the action of this loop is the reference DC current for the inverter. Another PI is used to regulate the current and generates the reference for the PWM loops as in Figure 2-18.

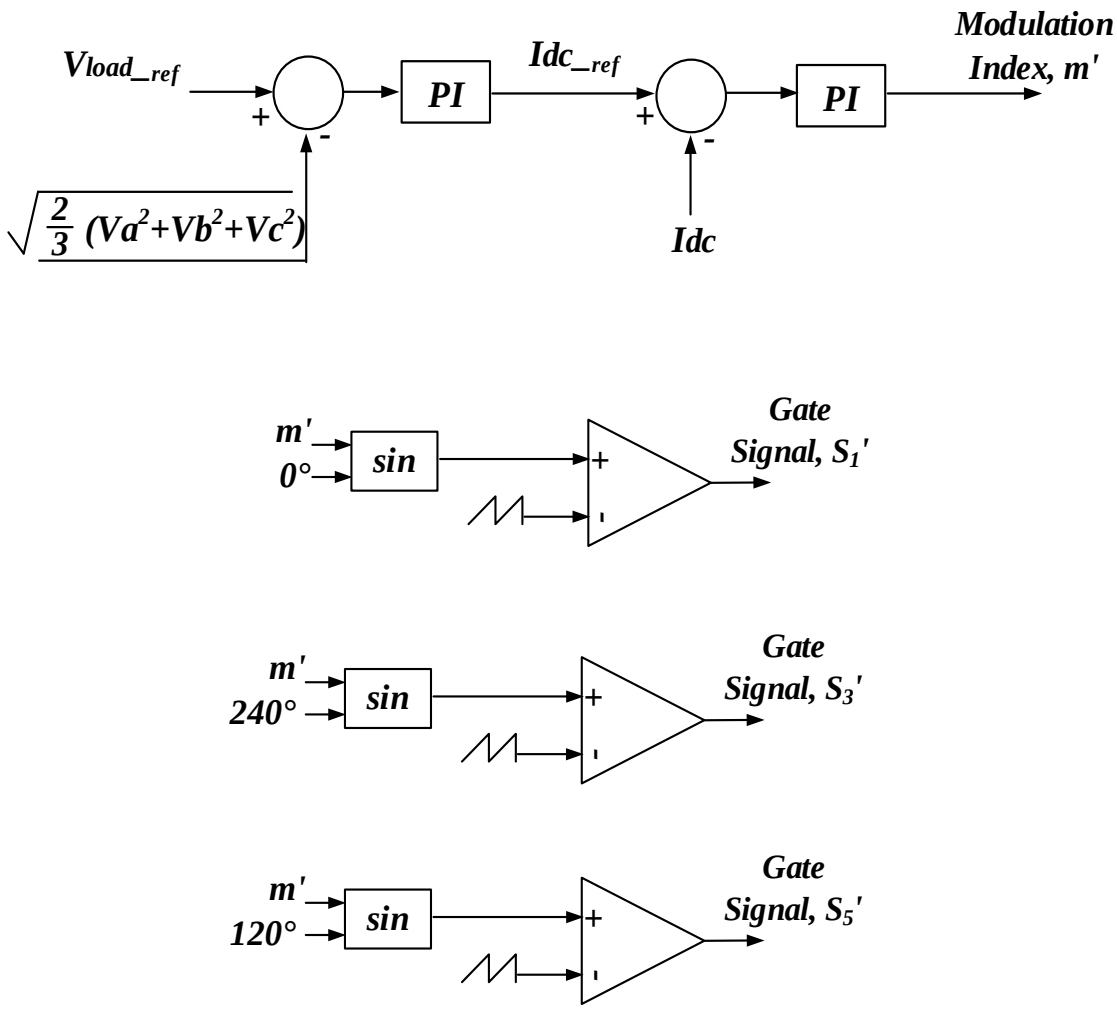

Figure 2-18: Control loop for the three phase inverter.

The reference vs actual peak load voltage, the input DC current, and the modulation index m′ for the inverter are shown in Figure 2-19 (a), (b), and (c) ; the controller was able to retain the value of the required load current even at the instant of step change.

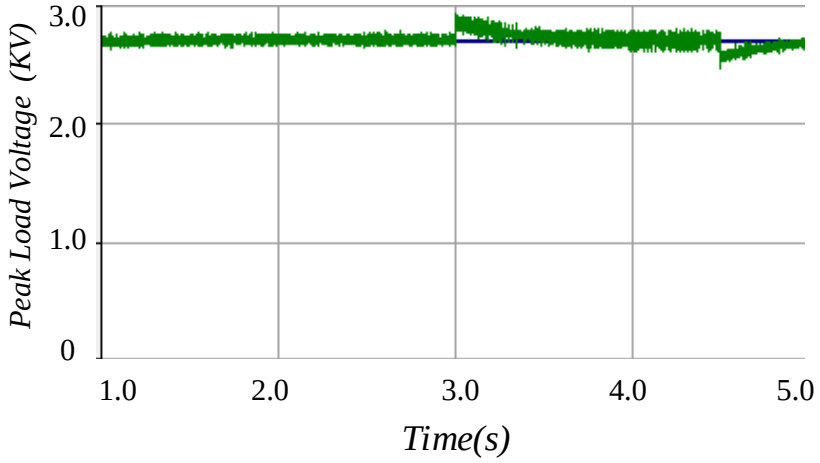

(a)

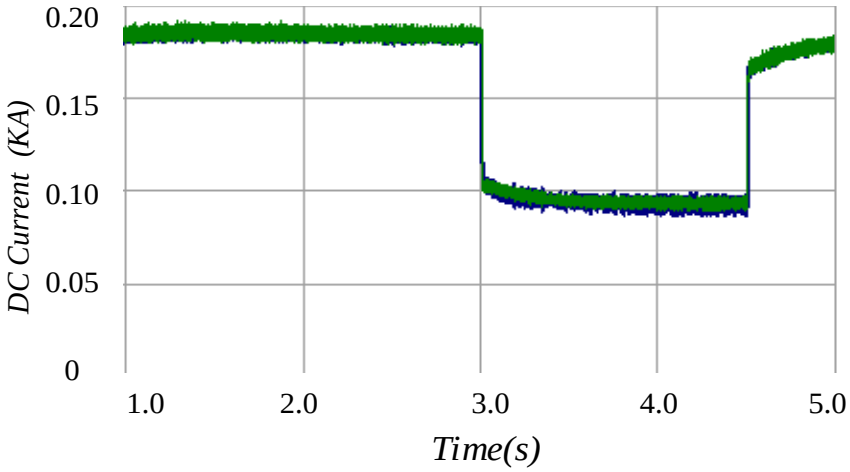

(b)

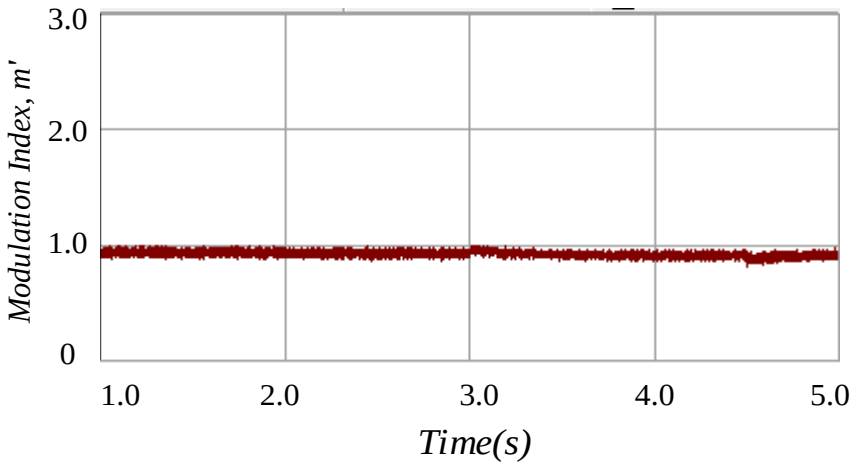

(c)

Figure 2-19: (a) Peak load voltage, (b) Input DC current for the inverter, and (c) modulation index m'.

The output AC load voltage and current are illustrated in Figure 2-20, the voltage and current are sinusoidal and in phase. At time=3s, a step change occurred in the resistive load, where the converter succeeded to track the desired output voltage value, while the output current change. The total harmonic distortion (THD) is < 0.5.

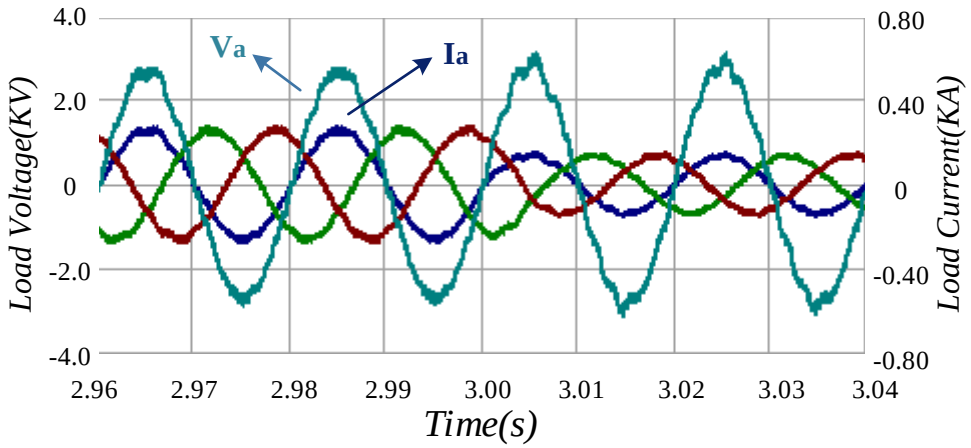

Figure 2-20: AC load voltage and current.

2.5.1 Grid Connected BTB Three Phase Buck-Boost Converter

The performance of the BTB converter is tested when connected to a 3.3 KV grid as shown in Figure 2-21.

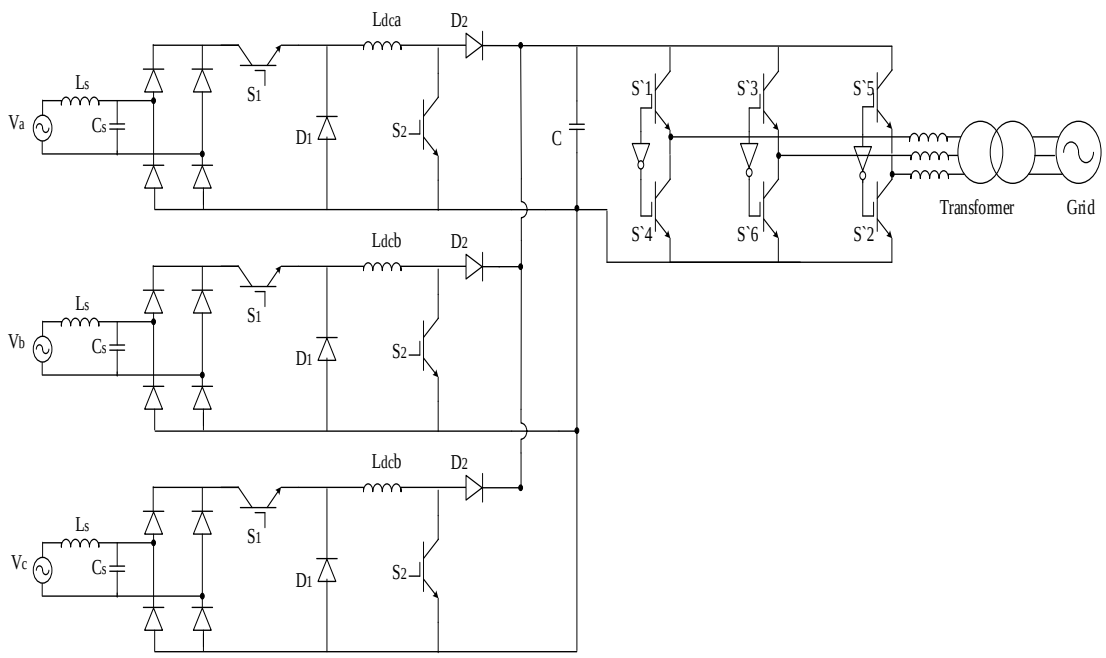

Figure 2-21: Three phase BTB grid connected converter.

The gate signal for the buck-boost converter is obtained using Figure 2-17. For the gating signals of the inverter, the vector control is used by transforming the grid voltage and current from the abc to the dqo frame using the Park's transformations. Figure 2-22 shows the space vector angle theta for park's transformation which is obtained using phase locked loop (PLL) [46].

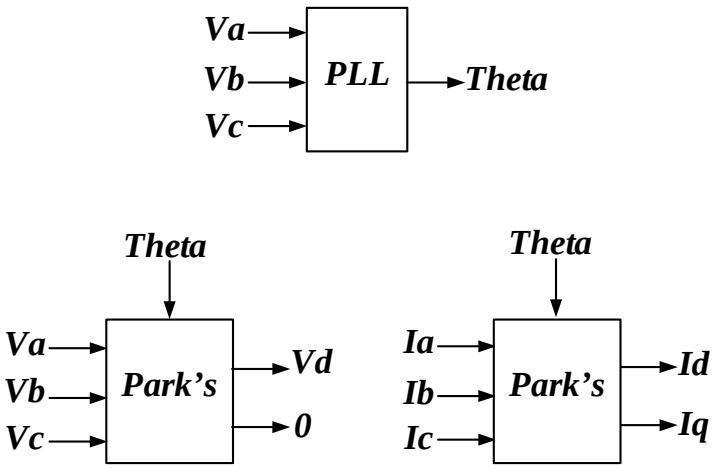

Figure 2-22: PLL for the grid voltage and current.

A PI is used to regulate the grid active power at reference value 1MW, followed by another one to control the grid's direct current component, i_d. The grid's reactive power is set to zero using a PI controller as in Figure 2-23 to control the quadrature current component i_q.

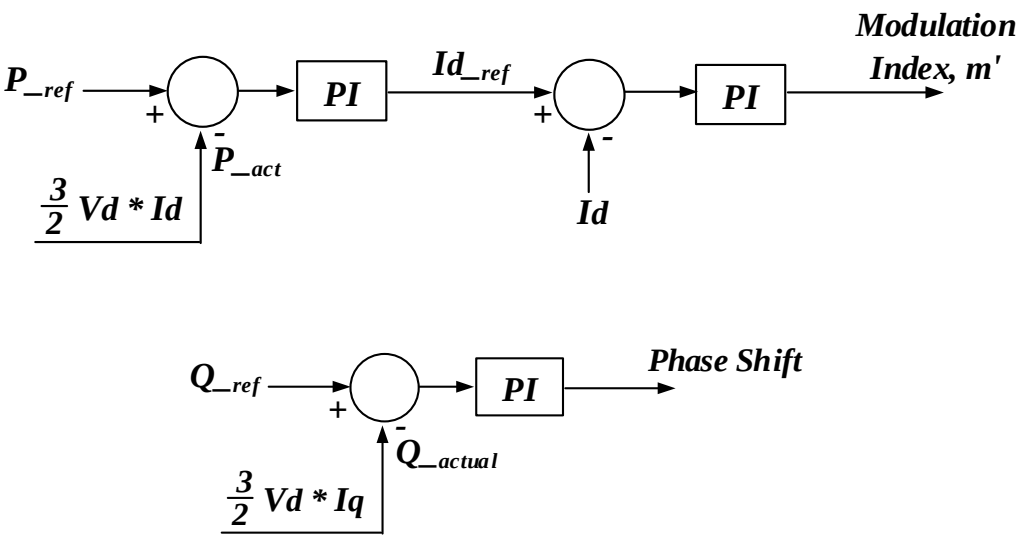

Figure 2-23: PWM technique for the three phase inverter.

The output of both loops from Figure 2-23 are used to obtain the three gating signal for the inverter's switches using a sinusoidal PWM technique as illustrated in Figure 2-24.

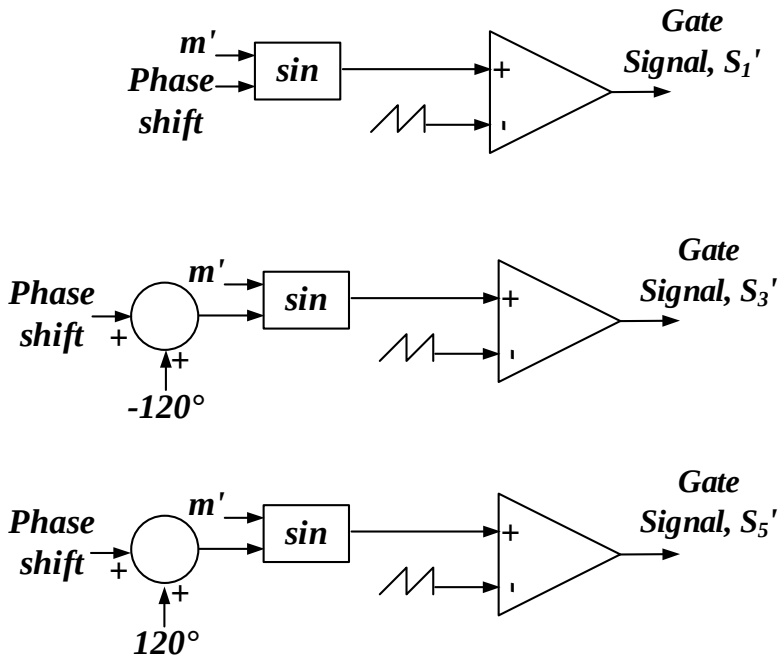

Figure 2-24: Gating signals for the three phase inverter.

The Grid voltage and current are demonstrated in Figure 2-25, where the voltage and current are sinusoidal and in phase.

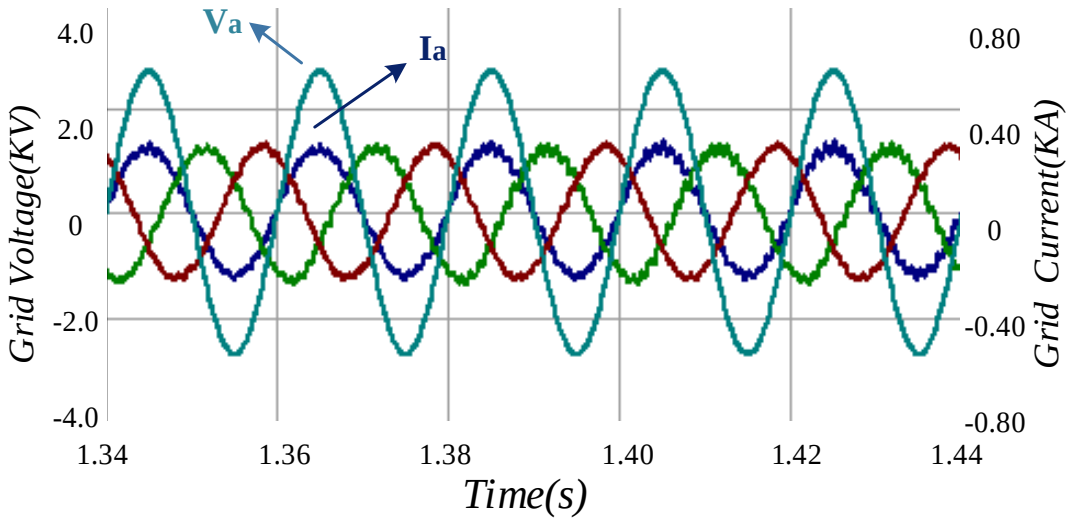

Figure 2-25: Three phase grid Voltage and Current.

Following their control loops in Figure 2-23, the grid active power is illustrated in Figure 2-26 (a) and the modulation index m′ in Figure 2-26(b). The reactive power and the phase shift angle are shown in Figure 2-27(a) and (b) respectively. The controller is able to regulate both powers at their reference value in milliseconds.

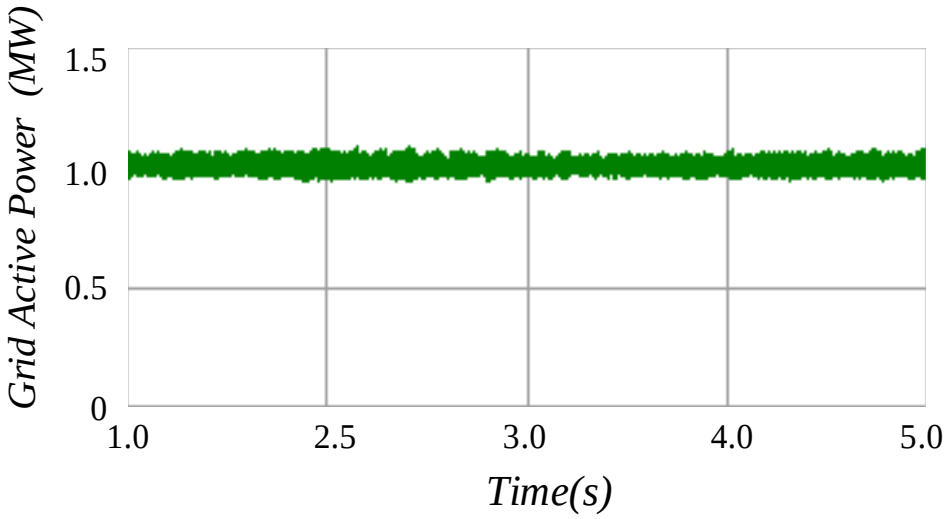

(a)

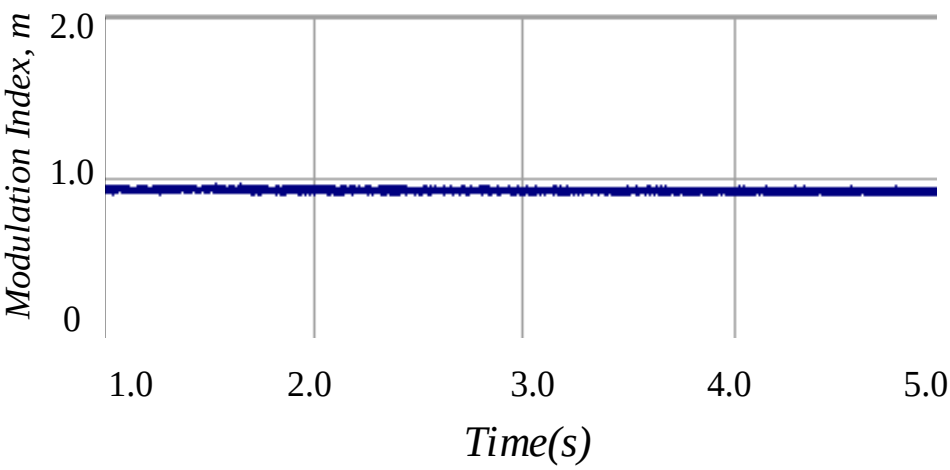

(b)

Figure 2-26: (a) Grid active power, (b) modulation index m′.

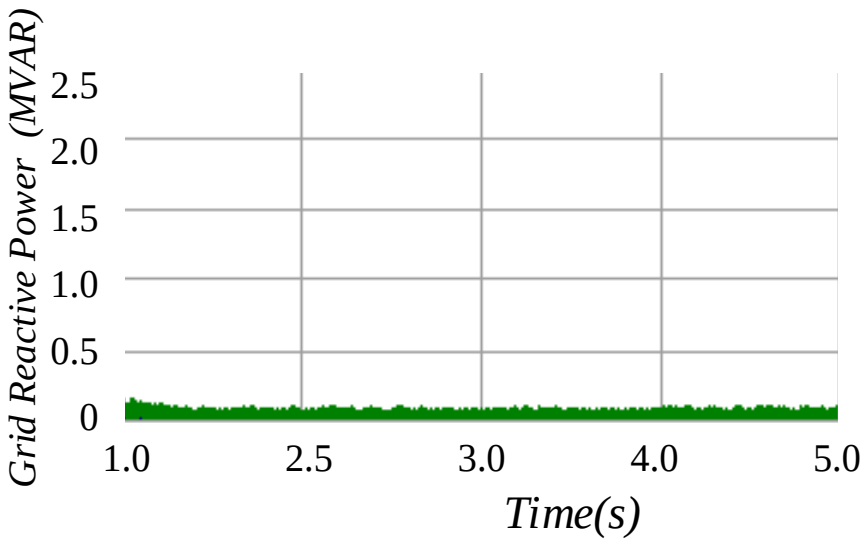

(a)

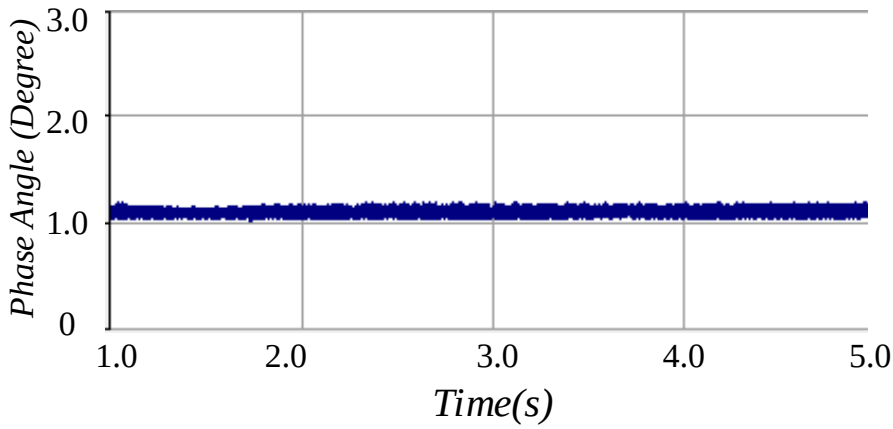

(b)

Figure 2-27: (a) Grid Reactive Power, (b) Phase angle.

Chapter Three

3 MODELLING OF THE PMSG BASED WECS

3.1 WIND TURBINE MODEL

WECS consists mainly of a wind turbine and an electrical generator to convert the kinetic energy into electrical energy, where the turbine is designed to deliver the mechanical power of the air flow around the blades to the rotor of the mounted generator [47], [48].

As HAWT is the most common used for producing more power, the kinetic energy of the air flow through area A can be determined through the following equation:

$$E = \frac{1}{2}\, m\, \vartheta^2 \tag{3.1}$$

Where m is the amount of air flow, ϑ is the wind speed, ρ is the air density (1.225 kg/m^3), r is the radius of the swept area, and A is the air swept area as shown in Figure 3-1 and can be calculated using the following relation:

$$A = \pi r^2 \tag{3.2}$$

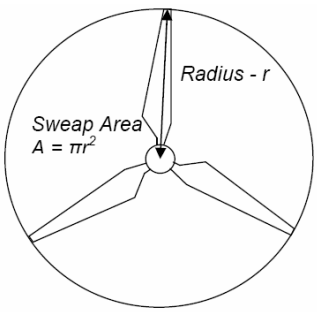

Figure 3-1: Total area swept by the blades [49]**.**

Therefore,

$$\frac{dm}{dt} = \rho\, A\, v \tag{3.3}$$

The power of the wind energy is defined as the rate of change of the kinetic energy per second:

$$Pwind = \frac{dE}{dt} = \frac{1}{2}\frac{dm}{dt}v^2 = \frac{1}{2}\rho\, A\, v^3 \tag{3.4}$$

The turbine is designed to deliver the mechanical power of the air flow around the blades to the rotor of the mounted generator, since it is hardly possible to obtain all the power from the wind. The aerodynamic power of the turbine is determined using a power coefficient Cp which is a function of the tip speed ratio λi and the blade pitch angle β as follows:

$$\mathrm{Cp} = 0.5176\left(\frac{116}{\lambda \mathrm{i}} - 0.4\beta - 5\right)\mathrm{e}^{\frac{-21}{\lambda \mathrm{i}}} - 0.006795\,\lambda \mathrm{i} \tag{3.5}$$

The power coefficient Cp is maximum at λ_{opt} which is calculated using:

$$\lambda \mathrm{i} = \left[\frac{1}{\lambda + 0.08\,\beta} - \frac{0.035}{\beta^3 + 1}\right] \tag{3.6}$$

$$\lambda = \frac{\mathrm{rw}}{\mathrm{v}} \tag{3.7}$$

Since v is the wind speed, and w is the rotor tip angular speed, the mechanical power of the turbine can be found from:

$$Pmech = Cp\, Pwind = \frac{1}{2}\rho\, A \quad Cp(\lambda, \beta)\vartheta^3$$

The mechanical torque of the turbine is calculated from:

$$T = \frac{P_{\mathrm{mech}}}{\mathrm{w}} = \mathrm{Cp}\frac{P_{wind}}{\mathrm{w}} = \frac{1}{2}\rho\, \mathrm{A}\, \mathrm{Cp}(\lambda, \beta)\frac{\mathrm{v}^3}{w} \tag{3.8}$$

3.1.1 WIND TURBINE CHRACTRASTIC

The value of Cp is a function of λ when the swept area of the blade and the air density are constant, and $\beta = 0°$. It is maximum at the particular value of λopt. By solving the previous equations using MATLAB it was found that Cp = 0.5 at λopt =8.1, which means that about 50.2% of the power can be extracted from the turbine as presented in Figure 3-2.

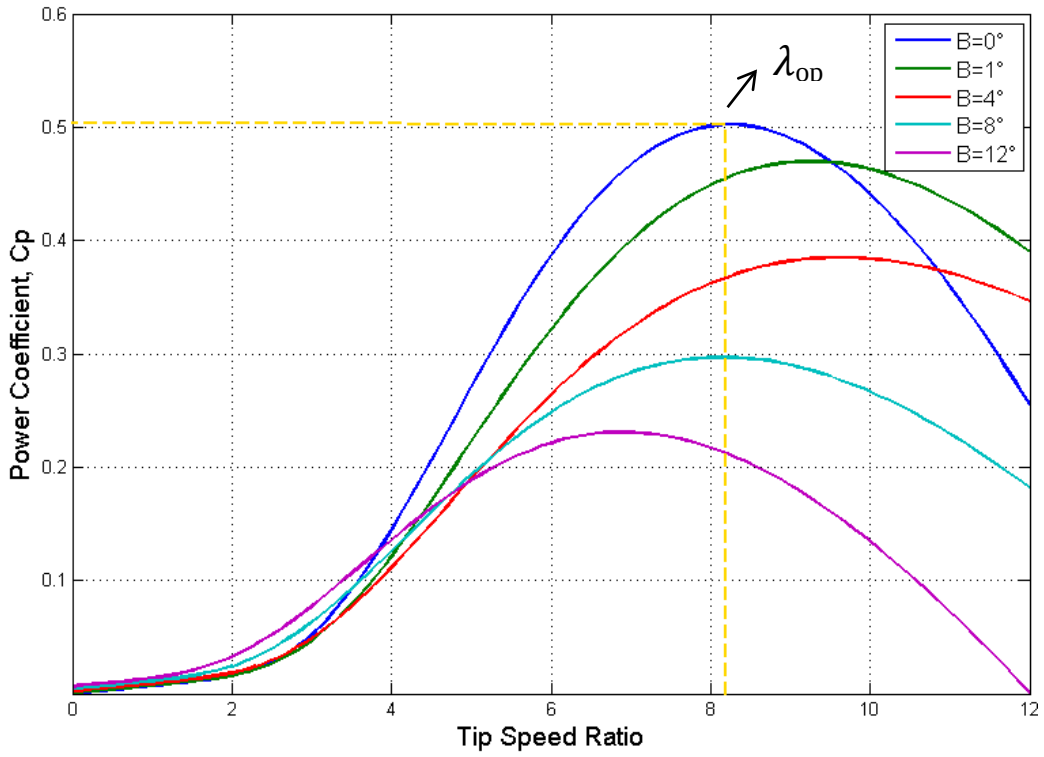

Figure 3-2: The power coefficient vs. tip speed ratio at different pitch angle.

To find the maximum power point, Figure 3-3 shows the active power of the wind turbine at different wind speeds, where the maximum wind speed is 12.5 m/s.

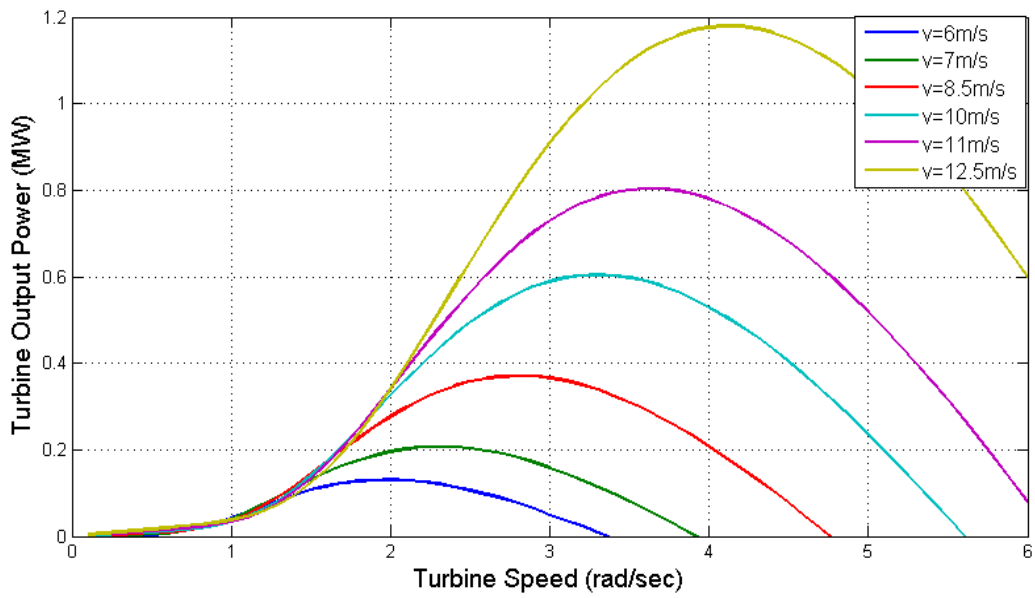

Figure 3-3: Wind turbine active power at different wind speed.

3.2 PMSG

Permanent magnet synchronous generator is a synchronous machine, where the magnetization is done using permanent magnets placed on the rotor instead of using coils for dc excitation. The usage of permanent magnets makes the PMSG a brushless machine which reduces the weight of the generator, leading to an increase in the efficiency and reliability and can also reduce the thermal stress on the rotor. Another advantages for the PMSG is requiring less maintenance and can be connected directly to the turbine, without the need for a gearbox, when having a high number of poles [50].

3.2.1 Three Phase PMSG Model

The mathematical equations for an open winding three phase PMSG are obtained in the abc form then transformed using park's transformation matrix into the dqo form (direct axis and quadrature axis) [29], where the stator voltages V_{abc} is transferred into the rotating reference frame V_{dq} so as to simplify the calculations as in (3.9) and to ease the control of the machine. Figure 3-5 illustrate the dq rotating frame, where θ is the angle between a-axis and d-axis.

$$\begin{bmatrix} v_d \\ v_q \\ v_0 \end{bmatrix} = \frac{2}{3} \begin{bmatrix} cos\theta & cos\left(\theta - \frac{2\pi}{3}\right) & cos\left(\theta + \frac{2\pi}{3}\right) \\ -sin\theta & -sin\left(\theta - \frac{2\pi}{3}\right) & -sin\left(\theta + \frac{2\pi}{3}\right) \\ ½ & ½ & ½ \end{bmatrix} \begin{bmatrix} v_a \\ v_b \\ v_c \end{bmatrix} \tag{3.9}$$

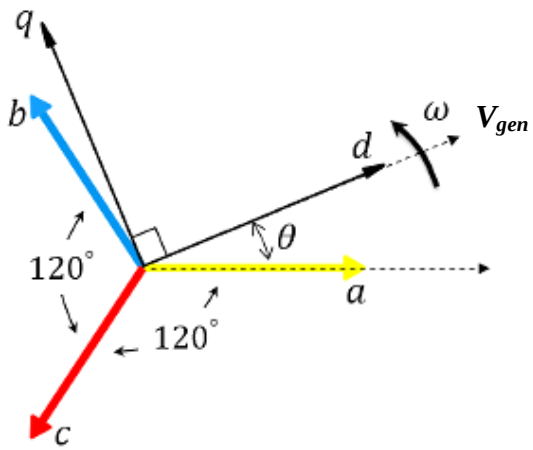

Figure 3-4:Three phase and rotating reference frame [51].

The PMSG model is similar to the standard synchronous generator except for the absence of dc field coil, where the excitation is provided by the permanent magnet giving a constant flux Ψ.

The inductance matrix $[L_{abc}]$ of the PMSG is given by [52], [53] :

$$[L_{abc}] = \begin{bmatrix} l_{aa} & l_{ab} & l_{ac} \\ l_{ba} & l_{bb} & l_{bc} \\ l_{ca} & l_{cb} & l_{cc} \end{bmatrix} \tag{3.10}$$

Where l_{aa} is the stator self-inductance of phase a, and l_{ab} is the stator mutual-inductance between phase a and b. The different inductances are given as follow:

$$l_{aa} = l_s + l_m cos2\theta \tag{3.11}$$

$$l_{bb} = l_s + l_m cos2(\theta - \frac{2\pi}{3})$$

$$l_{cc} = l_s + l_m cos2(\theta + \frac{2\pi}{3})$$

$$l_{ab} = l_{ba} = -M_s + l_m cos2(\theta - \frac{2\pi}{3})$$

$$l_{bc} = l_{cb} = -M_s + l_m cos2\theta$$

$$l_{ca} = l_{ac} = -M_s + l_m cos2(\theta + \frac{2\pi}{3})$$

The voltage equation in the abc frame is:

$$[v_{abc}] = -[R_s][i_{abc}] - p[\Psi_{abc}] \tag{3.12}$$

$$[\Psi_{abc}] = [L_{abc}]\,[i_{abc}] + [\,\Psi_{fs}] \tag{3.13}$$

Where, Ψ_{fs} is the flux linkage due to the existence of the permanent magnet.

$$[\Psi_{fs}] = \begin{bmatrix} \Psi_f\ cos\theta \\ \Psi_f\ cos\left(\theta - \frac{2\pi}{3}\right) \\ \Psi_f\ cos\left(\theta + \frac{2\pi}{3}\right) \end{bmatrix} \tag{3.14}$$

By substituting Equation (3.14), and (3.11) in (3.13), and in Equation (3.12), the voltage of the generator in the abc frame can be obtained. By applying park's transformation in (3.9), the voltage can be written in the dqo frame as follow:

$$v_d = -R_s i_d - p\Psi_d + \omega_e \Psi_q \tag{3.15}$$

$$v_q = -R_s i_q - p\Psi_q - \omega_e \Psi_d \tag{3.16}$$

$$\Psi_d = L_d i_d + \Psi_f \tag{3.17}$$

$$\Psi_q = L_q i_q \tag{3.18}$$

Where v_d and v_q are the direct and quadrature stator voltage components respectively, i_d and i_q are the stator current components, R_s the stator resistance, p is the operator of differentiation, ω_e is the electrical generator angular speed. L_d , and L_q are the d- and q- axis stator inductances [54].

The electromagnetic torque equation can be written as [55]:

$$T_e = \frac{3}{2}\left(\frac{P}{2}\right)\left(\Psi_f i_q + \left(L_d - L_q\right) i_q i_d\right) \tag{3.19}$$

And the electromechanical torque is given by:

$$T_e = J\left(\frac{2}{P}\right)\frac{d\omega_r}{dt} + \beta\omega_r\left(\frac{2}{P}\right) + T_L \tag{3.20}$$

Where J is the moment of inertia, β is the friction co-efficient, and T_L is the load torque.

Chapter four

4 SIMULATION RESULTS OF THE WECS

4.1 MODEL DISCRIPTION

A 1.1 MW wind turbine using a three-phase PMSG with an open-end winding connected to three buck-boost converters through three single phase parallel uncontrolled rectifiers. The buck-boost is controlled such that to achieve MPPT. The generator-side buck-boost converters are supplying a three-phase VSI through a common dc-link, consisting of a capacitor. The VSI is used to control the active and reactive power fed to the grid. The simulation is done using EMTDC/PSCAD software.

Schematic diagram of the proposed WECS is presented in Figure 4-1 and the simulated system is shown in Figure 4-2.

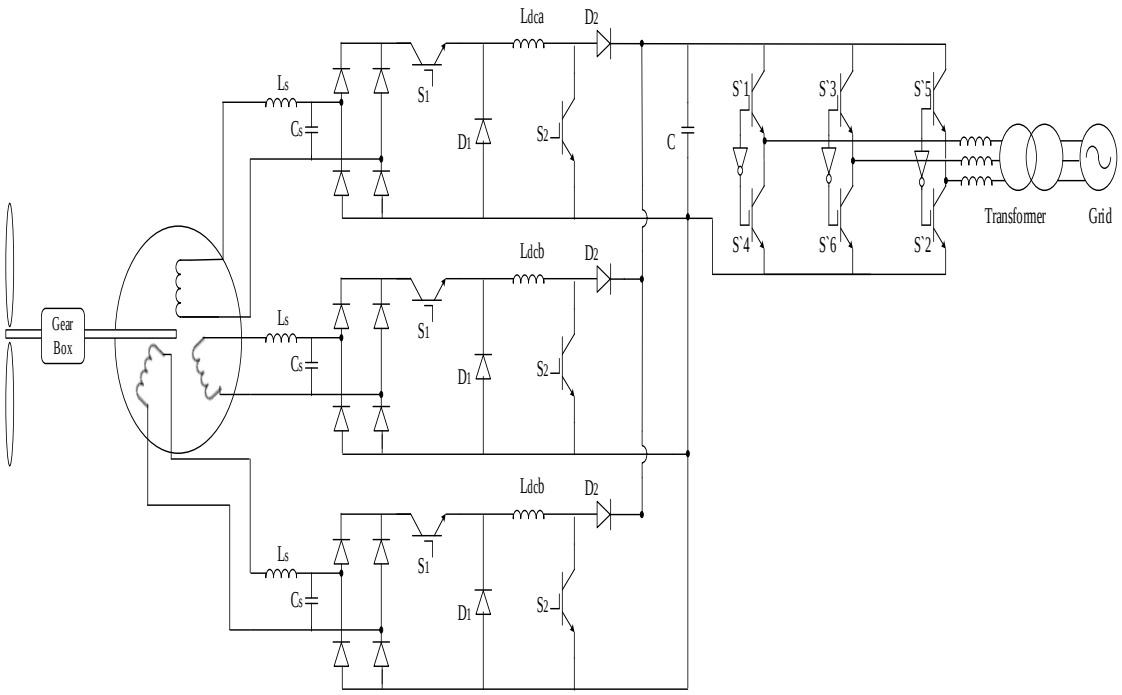

Figure 4-1: Proposed WECS diagram.

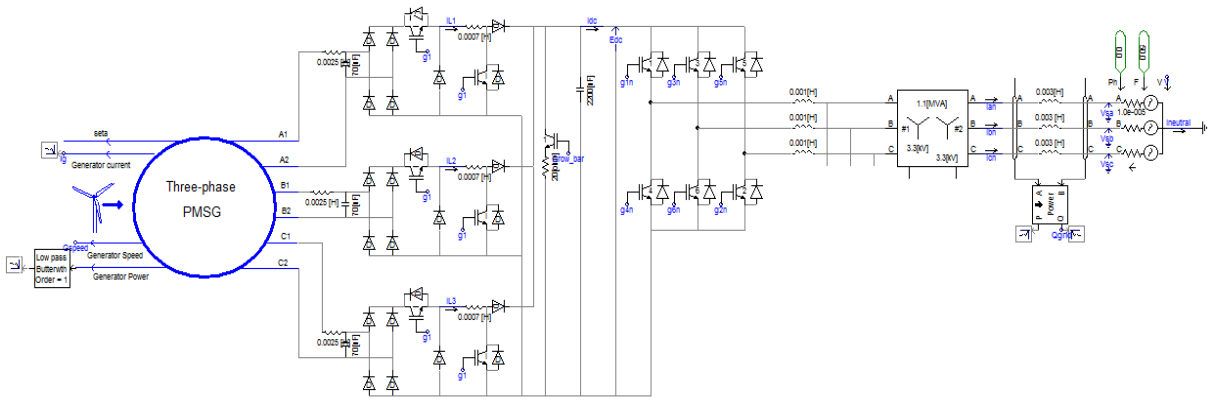

Figure 4-2: Proposed WECS schematic diagram using EMTDC/PSCAD.

4.2 BUCK-BOOST CONVERTER DESIGN

The design of the DC inductor for the three phase parallel AC-DC converter is obtained from [56] as follow:

$$L_{dc} < \frac{T_s\, V_{cap}(1-D)}{2 i_{cap}} \tag{4.1}$$

V_{cap} is the capacitor voltage, T_s is periodic switching time , D is the duty cycle and i_{cap} is the capacitor current.

4.2.1 MPPT Algorithm

The MPPT technique is required in order that the turbine is operated at its optimum tip speed ratio to get its maximum power at any variable wind velocity. The gating for the buck-boost converter is produced by two cascaded control loops. The outer control loop is dedicated for the MPPT while the inner loop controls the PMSG current.

To achieve MMPT, a PI controller is used to regulate the generator speed at its optimal reference. The action of this loop is the generator peak current reference which is the setting for the current control loop. The DCM results in sinusoidal input current to the ac-dc converter with unity power factor. The current control loop is based on a PI controller which set the duty cycle for the three buck-boost converters. The gate signal is generated using PWM technique.

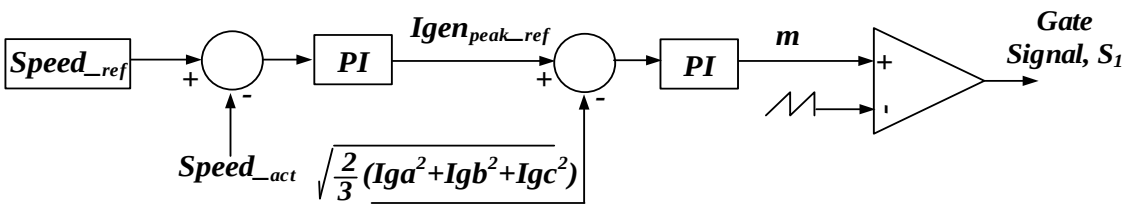

Figure 4-3: Proposed control loop of the buck-boost converter.

Figure 4-3 illustrates the control loop where the a PI controller is dedicated for the outer loop which compares the generator speed with the optimal reference speed then the output is compared to the peak value of the generator current to give the modulation index required for the saw tooth comparison of the PWM gate signal.

4.3 GRID SIDE VSI

A three-phase VSI is used to transfer the extracted active power from the PMSG by regulating the dc-link capacitor voltage and to control reactive power fed to the grid. It has a high power density reaching MVA where the switching frequency reaches KHZ; therefore the selected switches are IGBTs which has the advantages of being fast switches with high power rating. The switches of the VSI operate by comparing a modulating signal with a carrier signal which is called the carrier based PWM technique.

The aim of the GSC is to keep the DC link voltage constant despite of the generator output power, and support the grid reactive power during faults in order to fulfil the grid code requirements.

A PI controller is used to regulate the dc-link capacitor voltage by adjusting the grid's q-axis current, another PI is used to set the direct component of the reference current to inject zero reactive power to the grid during normal conditions as in Figure 4-4. The dq current components are transferred to abc frame using park's transformation with the aid of angle θ obtained from PLL.

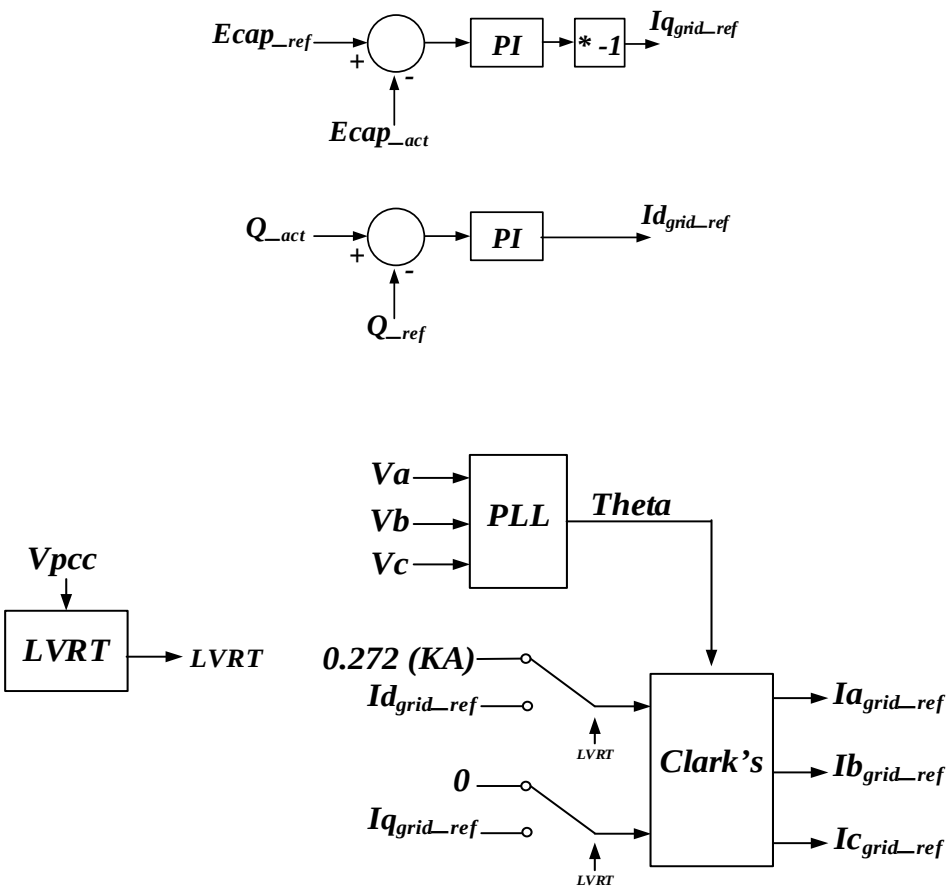

Figure 4-4: VSI control loops.

Then, a hysteresis current control is utilized to generate the switching signals for the VSI using the three phase grid actual current and reference current as in Figure 4-5.

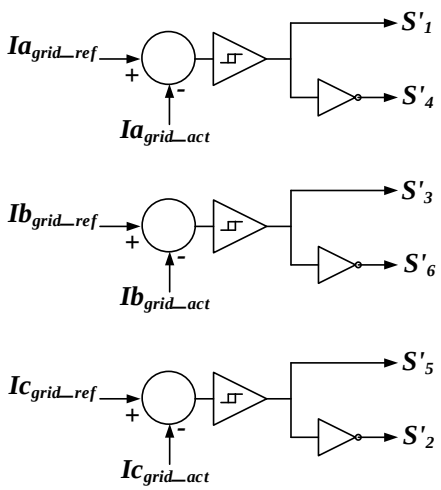

Figure 4-5: Hysteresis current control loops.

The VSI is feeding a 3.3 KV grid via a transformer where the power equations of the grid are obtained from [57]:

$$P_g = \frac{3}{2}(v_{dg}i_{dg} + v_{qg}i_{qg}) \tag{4.2}$$

$$Q_g = \frac{3}{2}(v_{qg}i_{dg} - v_{dg}i_{qg})$$

Aligning the grid voltage to the d-axis, results in v_{qg} equal to zero, therefore :

$$P_g = \frac{3}{2}v_{dg}i_{dg} \tag{4.3}$$

$$Q_g = -\frac{3}{2}v_{dg}i_{qg}$$

4.4 LVRT TECHNIQUE

For grid-connected wind farms, the WECS must attain grid code requirements under faulty conditions. Active or passive crowbar is utilized in case of voltage fluctuations due to grid faults, to shorten the generator's terminals [58], [59]. The active crowbar method used is based on a power electronic switch in series with a resistance.

The crowbar is connected across the dc-link capacitor and is turned-on once the dc-link capacitor voltage exceeds certain limit to discharge the capacitor and protect the back-to-back converter. The control for the VSI during LVRT is shown in Figure 4-4.

4.5 SIMULATION RESULTS

The simulation is done at three different wind speeds (6m/s, 12.5 m/s and 10m/s) to evaluate the dynamic performance of the proposed WECS scheme and its ability to track the maximum power at different operating conditions.

The system is also tested under grid voltage disturbance to evaluate the LVRT capability. The wind turbine and the PMSG parameters are listed in Table 1.

Table 4-1: Wind turbine and PMSG parameters.

Wind Turbine Parameters	
Rated power	1.1 MW
Rated wind speed	12.5 m/s
Rotor radius	26 m
Gear ratio	1:17
Cut in speed	4 m/s
Cut out speed	25 m/s
Air denisty	1.225 kg/m^3
PMSG Parameters	
Rated power	1.1 MW
Rated voltage	3.3 KV
Number of poles	6
Stator resistance	0.001 ohm
Direct-axis synchronous inductance	0.01 H
Quadrature-axes synchronous inductance	0.01 H
Number of poles	6
Permenant magnetic flux	4.7 wb

4.5.1 Normal Operating condition

The normal operation indicates the actions of both controllers for the machine side buck-boost converter and the grid side VSI. The generator actual speed and reference optimal speed are displayed in Figure 4-6. It can be observed that the proposed MPPT controller succeeded to regulate the PMSG speed at its reference speed value with minimum transient time.

As a result, the active power transferred to the grid is the maximum power extracted from the turbine as shown in Figure 4-7, and the reactive power equal zero.

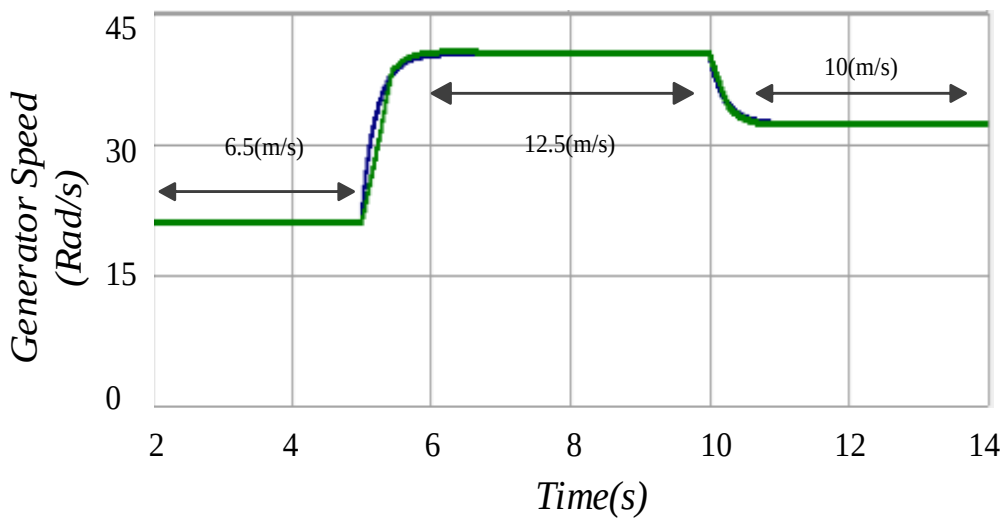

Figure 4-6: Generator speed and the optimal speed.

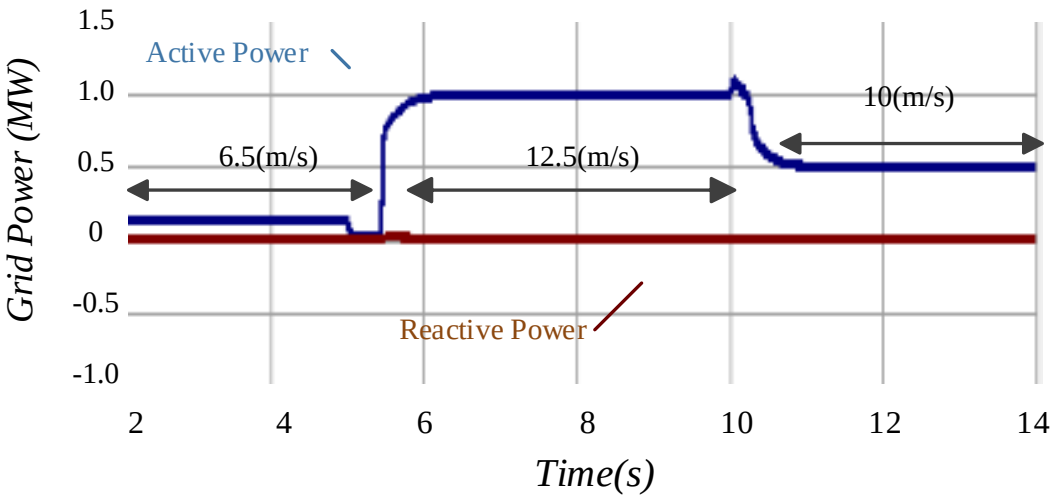

Figure 4-7: Grid active power and reactive power.

Figure 4-8 shows the peak value of the generator current and the reference value obtained from the outer loop of the control scheme as illustrated in Figure 4-3. The PI controller succeeded to regulate the value of the error in order to follow the different values of the wind speed.

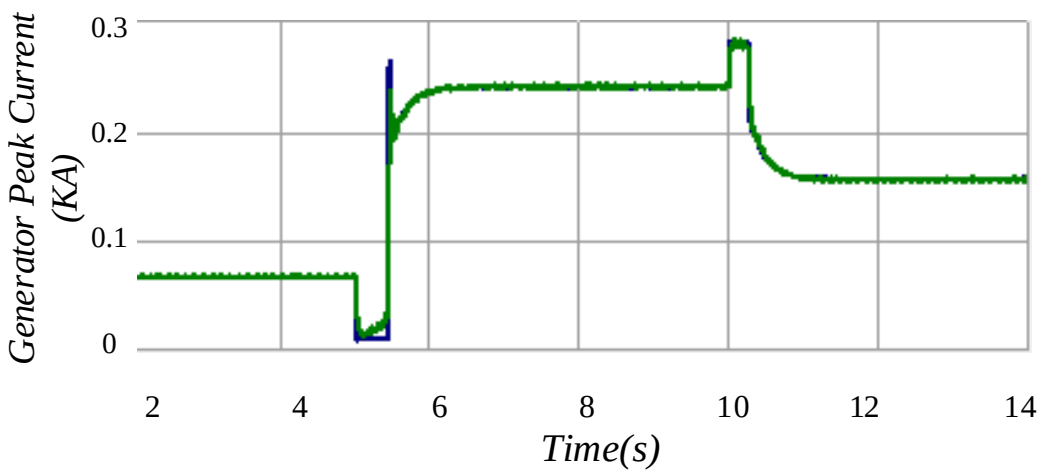

Figure 4-8: Generator peak current and the reference current.

The three-phase generator current is shown in Figure 4-9, where the currents are sinusoidal and shifted by 120°.

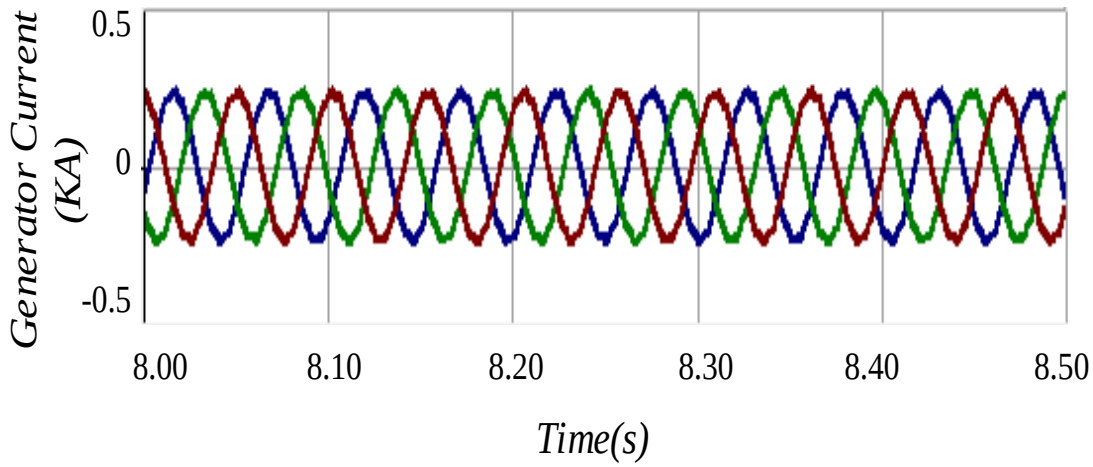

Figure 4-9: Three phase generator current.

Figure 4-10 illustrates the inductor current Ldc1 of the proposed buck-boost converter used for phase a. A zoom in is taken from Figure 4-10(a) in Figure 4-10(b) to demonstrate the DCM operation of the buck-boost converter. The inductor current is seen in three different states, where first the inductor is charging, then discharging, and finally the zero state.

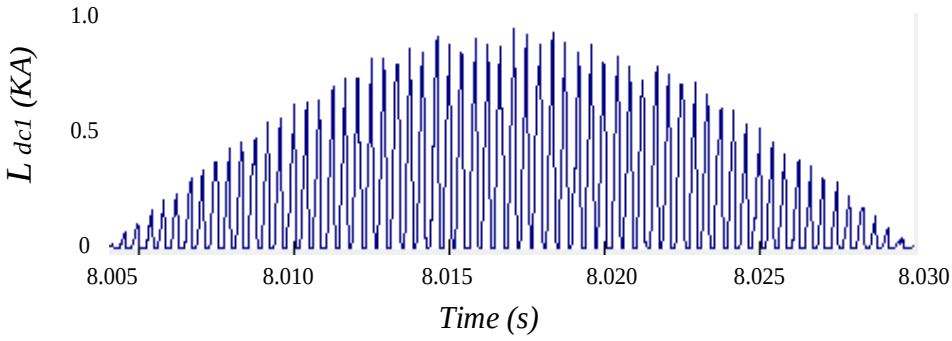

(a)

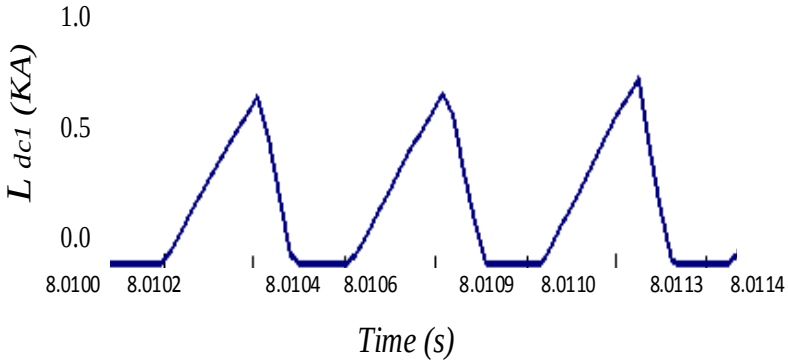

(b)

Figure 4-10: (a) Inductor current of the buck-boost and (b) Zoom in from (a).

The capacitor voltage of the DC link is shown in Figure 4-11, the voltage is kept constant at the different wind speeds.

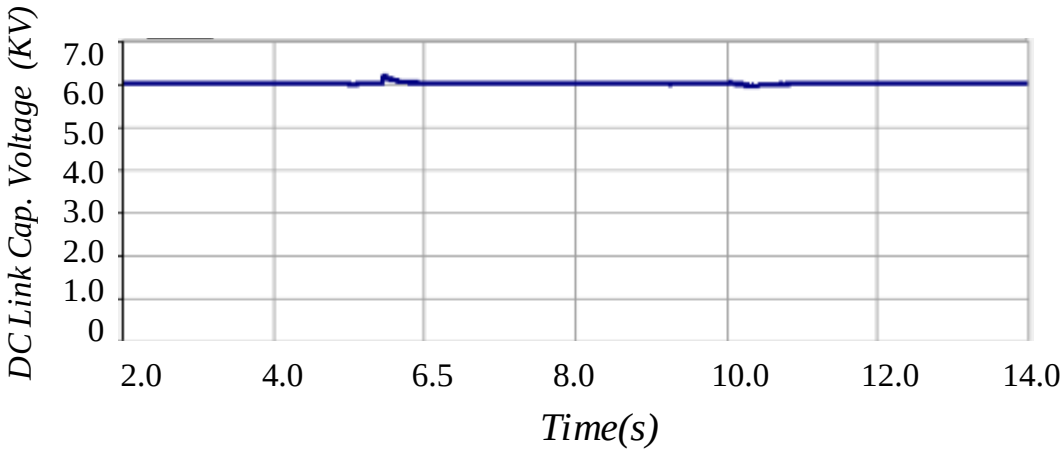

Figure 4-11: DC link capacitor voltage.

Figure 4-12 displays phase ‘a’ of the grid voltage and the grid current where the VSI controller is capable of delivering sinusoidal current and voltage to the grid.

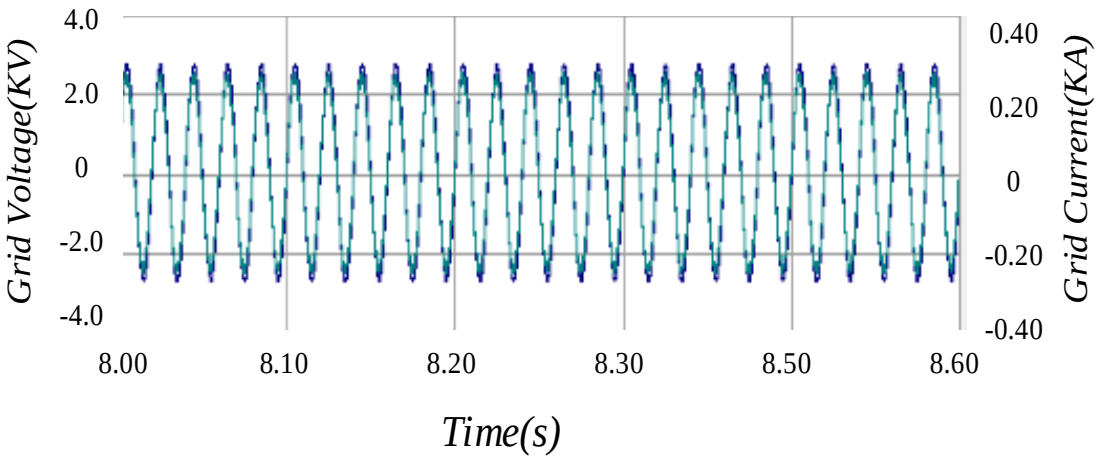

Figure 4-12: Grid voltage and current.

4.5.2 Operation under Grid Fault

The proposed WECS system is examined for a 150ms grid fault, which is initiated at *t*=2s when the wind speed is 12.5m/s.

Figure 4-13 illustrates the behaviour of the system during the fault. The active power generated from the PMSG and the active powers fed to grid are shown in Figure 4-13(a). It is noticed that the generator active power falls to half its rated value due to the reduction in the grid voltage.

Figure 4-13(b) and Figure 4-13(c) illustrate the dc-link capacitor voltage and the generator speed, respectively. During the fault, the grid voltage falls down while the wind turbine is still operating and connected to the grid where the VSI fails to supply the grid with the active power produced by the generator. As a result, an increase in the generator speed can be noticed during the fault, as well as a slight increase in the capacitor voltage. The crowbar is activated when the capacitor voltage rises to a certain limit to maintain the dc-link capacitor voltage within an acceptable limit.

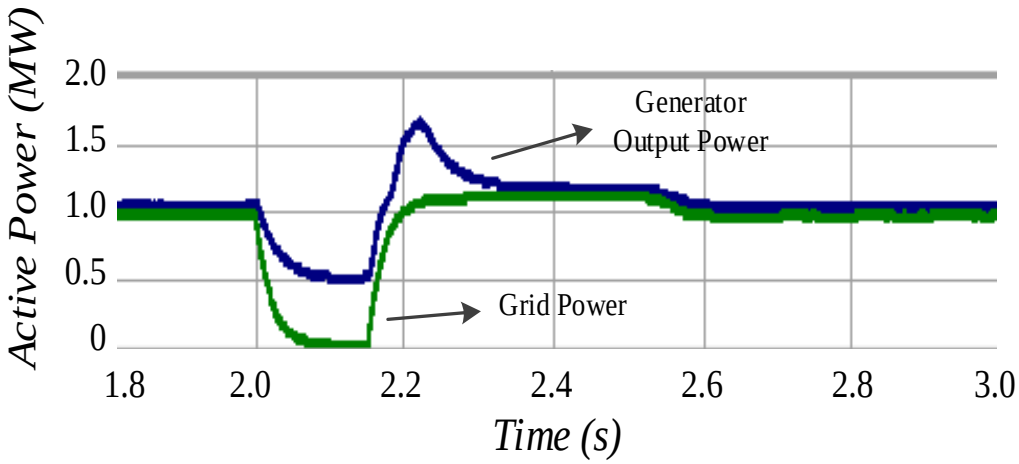

(a)

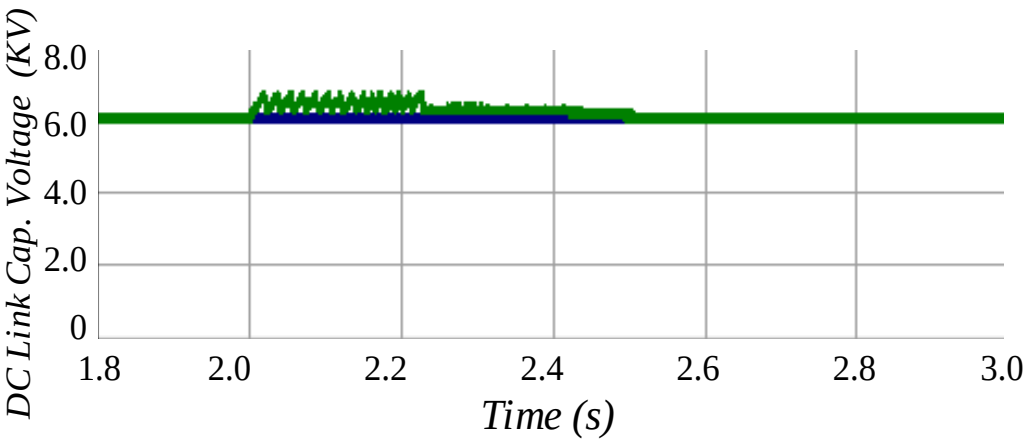

(b)

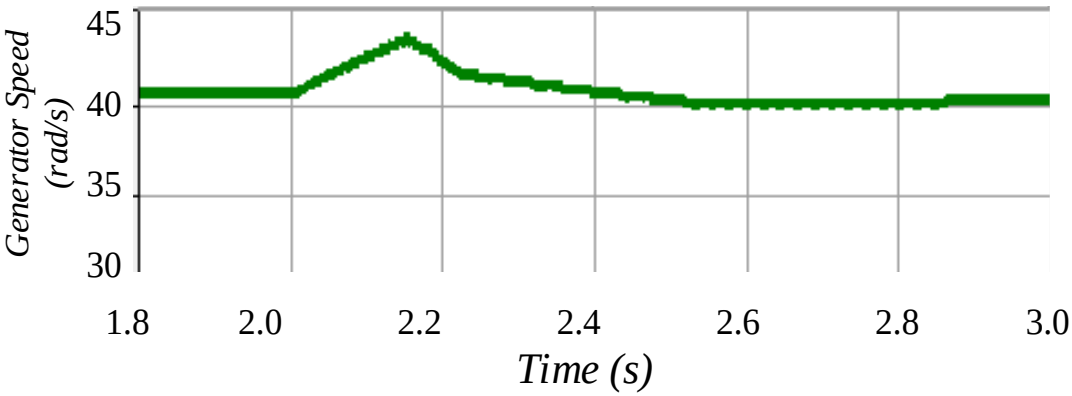

(c)

Figure 4-13: LVRT capability (a) Active powers, (b) DC link capacitor voltage, (c) Generator speed.

The reference direct and quadrature current of the VSI are shown in Figure 4-14 (a) and (b) respectively. At the instant of fault, the direct current is equal to the grid rated current to inject reactive current to the grid, while the quadrature current is equal to zero as shown in figure 4-4.

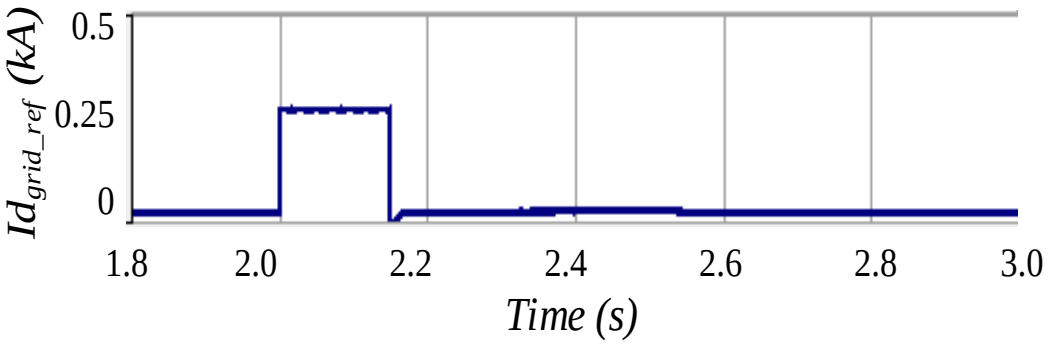

(a)

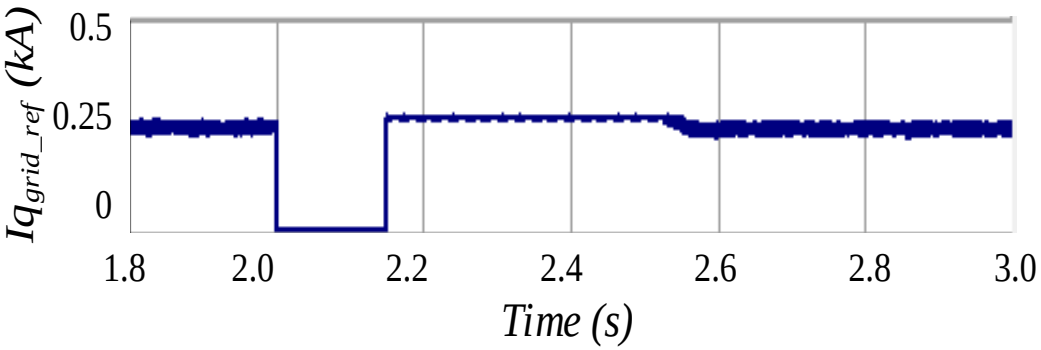

(b)

Figure 4-14: (a) the reference direct current , (b) the reference quadrature current.

The proposed scheme succeeds to deliver sinusoidal current in-phase with the supply voltage. During the grid fault, the proposed LVRT controller was able to deliver the rated reactive current and once the fault is cleared, the proposed controller again succeeds to return back to its normal operating condition with minimum transient time as observed in Figure 4-15, which shows phase ‘a’ of the grid voltage and the line current.

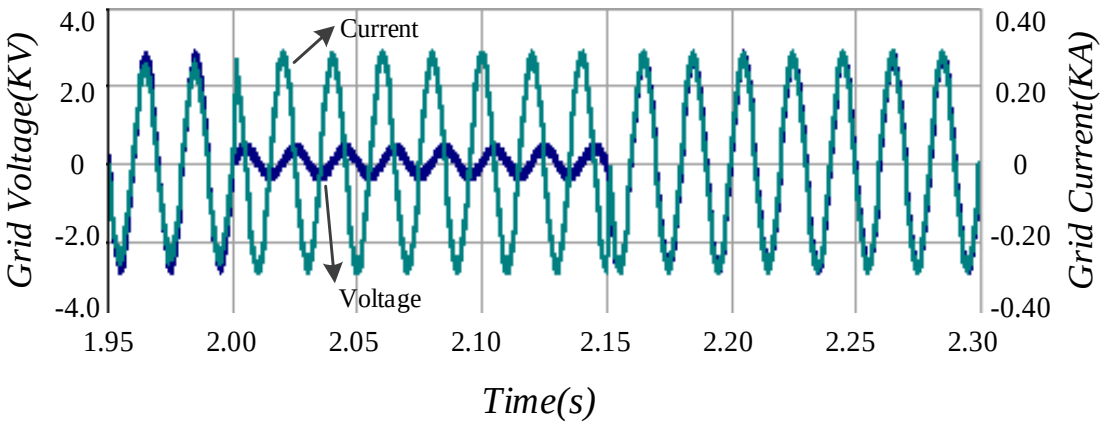

Figure 4-15: Grid voltage and current during fault.

It is visible that the proposed control succeeds to keep the sinusoidal shape of the PMSG currents even during the grid fault as indicated in Figure 4-16.

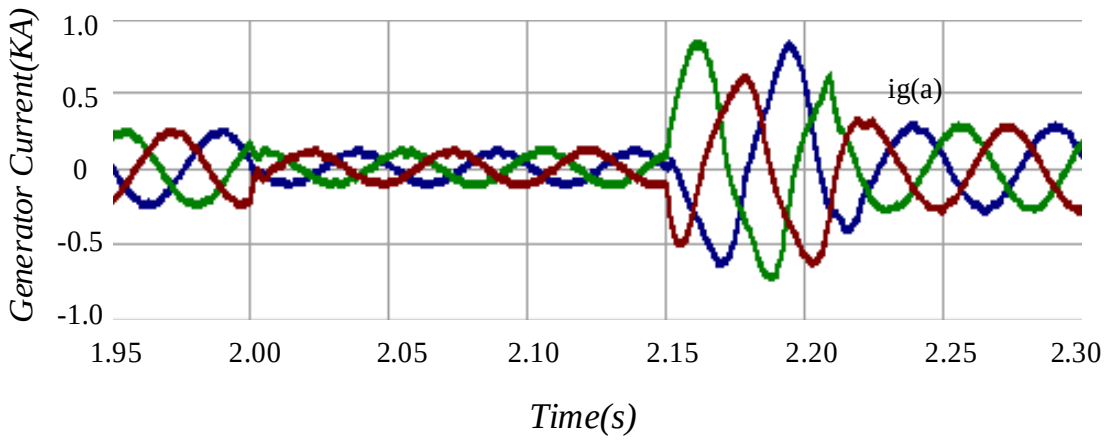

Figure 4-16: Three phase generator current during fault.

Chapter five

5 CONCLUSION

The introduced buck-boost converter's dynamic performance is tested under several conditions. Firstly, the AC-DC converter is examined when applying single phase supply voltage using a single phase uncontrolled rectifier where the controller succeeded to follow the output voltage reference value. The proposed three phase AC-DC converter is tested for a DC load to adjust the output DC voltage.

Moreover, the three phase converter is applied for the purpose of BTB converter applications. The performance of the islanded BTB converter with a step load change is achieved using a VSI where the control loops for both converters was able to track the load voltage. Furthermore, the grid connected BTB converter is examined.

The WECS based on three buck-boost dc-dc convertors operating in the DCM to interface the PMSG with the grid-connected VSI is introduced. The MPPT is used to regulate the speed by manipulating currents of the PMSG trough controlling the duty-ratio of the proposed ac-dc buck-boost converters. Moreover, a LVRT strategy based on active crowbar is integrated with the proposed scheme while the GSC is controlled to regulate the DC-link voltage and transfer the extracted active power to grid. Vector control is used for the VSI used for the GSC.

The simulation results using PSCAD/EMTDC verifies the operation of the proposed system under normal and fault conditions. The proposed control topology succeeds to extract the maximum power while operating the generator converter under DCM. In addition, the PMSG current is sinusoidal even during grid faults.

Future work:

1) Experiential implementations of the proposed rhythm to verify the dynamic performance.
2) Use an advanced controller instead of PI to enhance the performance.

LIST OF REFERENCES

[1] Y. Errami, M. Maaroufi, and M. Ouassaid, “Modelling and control strategy of PMSG based variable speed wind energy conversion system,” *Multimed. Comput. Syst. (ICMCS), 2011 Int. Conf.*, no. 2, pp. 1–6, 2011.

[2] M. I. Marei, A. Mohy, and A. A. El-sattar, “Electrical Power and Energy Systems An integrated control system for sparse matrix converter interfacing PMSG with the grid,” *Int. J. Electr. POWER ENERGY Syst.*, vol. 73, pp. 340–349, 2015.

[3] A. M. Update, *GWEC Global Wind Report_April 2018_Final*. 2017.

[4] G. S. Report, *Renewables 2017 global status report 2017*. 2017.

[5] M. A. Parker, C. Soraghan, and A. Giles, “Comparison of Power Electronics Lifetime Between Vertical- and Horizontal-Axis Wind Turbines,” *IET Renew. Power Gener.*, vol. 10, no. 5, pp. 679–686, 2015.

[6] B. Hughes and C. H N, “Computational Analysis of Dyanmic Architecture,” *J. power energy*, vol. 225, pp. 85–95, 2010.

[7] H. L. Z. Chen, “Overview of different wind generator systems and their comparisons,” *IET Renew. Power Gener.*, vol. 2, no. 2008, pp. 123–138, 2008.

[8] H. Polinder *et al.*, “Trends in Wind Turbine Generator Systems,” *IEEE J. Emerg. Sel. Top. Power Electron.*, vol. 1, no. 3, pp. 174–185, 2013.

[9] A. D. Hansen and L. H. Hansen, “Wind Turbine Concept Market Penetration over 10 Years (1995–2004),” *Wind Energy*, vol. 10, pp. 81–97, 2007.

[10] B. Kedjar, K. Al-haddad, F. Member, and P. Electronics, “Optimal Control of a Grid Connected Variable Speed Wind Energy Conversion System Based on Squirrel Cage Induction Generator,” *IECON 2012 - 38th Annu. Conf. IEEE Ind. Electron. Soc.*, pp. 3560–3565, 2012.

[11] S. Mali, S. James, and I. Tank, “Improving low voltage ride-through capabilities for grid connected wind turbine generator,” *Energy Procedia*, vol. 54, pp. 530–540, 2014.

[12] M. R. Banaei and A. R. Dehghanzadeh, “Wind Farm Based Doubly Fed Induction Generator Using a Novel AC / AC Converter,” pp. 398–402, 2011.

[13] S. K. B. Wu, Y. Lang, N. Zargari, *Power Conversion and Control of Wind Energy Systems*. NJ: Wiley, 2011.

[14] A. Bennouk, A. Nejmi, and M. Ramzi, “Stability Enhancement of a Wind Plant Based on a DFIG and a PMSM : A Lyapunov Approach,” *Energy Reports ELSEVIER*, vol. 4, pp. 13–22, 2018.

[15] T. De Paula Machado Bazzo, J. F. Kolzer, R. Carlson, F. Wurtz, and L. Gerbaud, “Multidisciplinary design optimization of a direct-drive PMSG including the power

converter cost and losses," *Proc. - 2016 22nd Int. Conf. Electr. Mach. ICEM 2016*, pp. 1909–1914, 2016.

[16] A. Sudhakaran and A. T.S, "Permanent Magnet Synchronous Wind Generator for Microgrid Dynamic Performance Improvement," *Int. Conf. Microelectron. Commun. Renew. Energy*, p. 6, 2013.

[17] A. E.- Bardawil and M. F. Moussa, "Power Management of Open Winding PM Synchronous Generator for Unbalanced Voltage Conditions," *J. Power Electron.*, vol. 16, no. 6, pp. 2192–2201, 2016.

[18] D. Zhou and F. Blaabjerg, "Comparison of Wind Power Converter Reliability With Low-Speed and Medium-Speed Permanent-Magnet Synchronous Generators," *IEEE Trans. Ind. Electron.*, vol. 62, no. 10, pp. 6575–6584, 2015.

[19] "National Grid ESO." [Online]. Available: https://www.nationalgrideso.com/codes/grid-code.

[20] L. Hudson, "The Serviced Grid Code," *Natl. Grid House*, vol. 14, no. 5, pp. 1–100, 2015.

[21] A. Etxegarai, P. Eguia, E. Torres, A. Iturregi, and V. Valverde, "Review of Grid Connection Requirements for Generation Assets in Weak Power Grids," *Renew. Sustain. Energy Rev.*, vol. 41, pp. 1501–1514, 2015.

[22] M. Draganescu, Y. Li, and S. Miao, "Review of Voltage and Frequency Grid Storage Applications," *Energies*, vol. 11, no. 5, pp. 1–26, 2018.

[23] M. Abdelrahem and R. Kennel, "Fault-Ride through Strategy for Permanent-Magnet Synchronous Generators in Variable-Speed Wind Turbines," *Energies*, vol. 9, no. 12, pp. 1–15, 2016.

[24] T. Heir, "The Serviced Grid Code," *Natl. Grid House*, vol. 21, no. 5, pp. 1–114, 2017.

[25] M. Nasiri, J. Milimonfared, and S. H. Fathi, "A review of low-voltage ride-through enhancement methods for permanent magnet synchronous generator based wind turbines," *Renew. Sustain. Energy Rev.*, vol. 47, pp. 399–415, 2015.

[26] R. Mittal, K. S. Sandhu, and D. K. Jain, "Low Voltage Ride-Through (LVRT) of Grid Interfaced Wind Driven PMSG," *ARPN J. Eng. Appl. Sci.*, vol. 4, no. 5, pp. 73–83, 2009.

[27] J. Chen and L. Jiang, "Perturbation Estimation Based Nonlinear Adaptive Control of a Full-Rated Converter Wind Turbine for Fault Ride-Through Capability Enhancement," *IEEE Power Energy Soc. Gen. Meet.*, pp. 1–11, 2015.

[28] B. Hoseinzadeh, F. Faria, D. Silva, and C. L. Bak, "Improved LVRT Grid Code under Islanding Condition," *IECON 2015 - 41st Annu. Conf. IEEE Ind. Electron. Soc.*, pp. 421–426, 2015.

[29] S. M. Muyeen, R. Takahashi, and T. Murata, "A Variable Speed Wind Turbine Control Strategy to Meet Wind Farm Grid Code Requirements," *IEEE Trans. Power Syst.*, vol.

25, no. 1, pp. 331–340, 2010.

[30] R. M. M. Pereira, A. J. C. Pereira, C. M. Ferreira, and F. P. M. Barbosa, “Influence of Crowbar and Chopper Protection on DFIG during Low Voltage Ride Through,” *Energies*, vol. 11, no. 4, p. 885, 2018.

[31] H. Geng, L. Liu, and R. Li, “Synchronization and Reactive Current Support of PMSG based Wind Farm during Severe Grid Fault,” *IEEE Trans. Sustain. Energy*, vol. 9, no. 4, pp. 1596–1604, 2018.

[32] O. Naghash, V. Fereshtehpoor, M. Hassan, and F. Blaabjerg, “Analysis , control and design of a non-inverting buck-boost converter : A bump-less two-level T – S fuzzy PI control,” *ISA Trans. ELSEVIER*, vol. 67, pp. 515–527, 2016.

[33] N. Zhang, G. Zhang, and K. W. See, “Systematic Derivation of Dead-Zone Elimination Strategies for the Non-Inverting Synchronous Buck-Boost Converter,” *IEEE Trans. Power Electron.*, vol. 33, no. 4, pp. 3497–3508, 2017.

[34] A. K. Chauhan, V. R. Vakacharla, A. K. Verma, and S. K. Singh, “Multiple PMSG fed Non-Inverting Buck-Boost Converter for HEVs,” in *2016 IEEE 6th International Conference on Power Systems (ICPS), New Delhi*, 2016, no. 1, pp. 1–6.

[35] D. Holliday, G. P. Adam, B. W. Williams, and I. Abdelsalam, “Single-stage ac–dc buck–boost converter for medium-voltage high-power applications,” *IET Renew. Power Gener.*, vol. 10, no. 2, pp. 184–193, 2016.

[36] I. Abdelsalam, G. P. Adam, D. Holliday, and B. W. Williams, “An improved single-phase AC-DC buck-boost converter operating in a discontinuous conduction mode,” *IET Conf. Publ.*, vol. 2016, no. CP684, pp. 1–6, 2016.

[37] J. Hussain, S. Member, M. K. Mishra, and S. Member, “Adaptive Maximum Power Point Tracking Control Algorithm for Wind Energy Conversion Systems,” *IEEE Trans. Energy Convers.*, vol. 31, no. 2, pp. 697–705, 2016.

[38] A. Tahri, H. Said, and S. Moreau, “A Robust Control for Permanent Magnet Synchronous Generator Associated with Variable Speed Wind Turbine,” *J. Electr. Eng.*, vol. 15, no. 2, pp. 1–8, 2015.

[39] K. Arora, “Control Analysis of PMSG based Wind Energy Conversion System using Buck-Boost Converter,” in *2016 Second International Conference on Computational Intelligence & Communication Technology*, 2016, pp. 395–402.

[40] Z. Zarkov, I. Bachev, and V. Lazarov, “Small Wind Generator System with Non-Inverting Buck-Boost Converter and Battery Storage,” in *15th International Conference on Electrical Machines, Drives and Power Systems (ELMA), Sofia*, 2017, pp. 283–303.

[41] V. Yaramasu and B. Wu, “Predictive Control of Three-Level Boost Converter and NPC Inverter for High Power PMSG-Based Medium Voltage Wind Energy Conversion Systems,” *IEEE Trans. Power Electron.*, vol. 29, no. 10, pp. 5308–5322, 2014.

[42] Y. Xia, K. H. Ahmed, and B. W. Williams, “Wind Turbine Power Coefficient Analysis of a New Maximum Power Point Tracking Technique,” *IEEE Trans. Ind. Electron.*, vol. 60, no. 3, pp. 1122–1132, 2013.

[43] A. Prabha, A. V Soumya, M. Baselious, and E. Trivandrum, “Improving the Performance of a Variable Speed Wind Pump With Z Source Inverter,” *2014 Int. Conf. Adv. Green Energy*, pp. 174–178, 2014.

[44] S. Pragaspathy, “A Review on DC-DC Converters for PMSG based Standalone Variable Speed Wind Turbine System,” vol. 5, no. 09, pp. 41–46, 2016.

[45] S. Lale, M. Soja, S. Lubura, D. Mancic, and M. Radmanovic, “A non-inverting buck-boost converter with an adaptive dual current mode control,” *Facta Univ. - Ser. Electron. Energ.*, vol. 30, no. 1, pp. 67–80, 2017.

[46] M. I. Marei and H. El-goharey, “Modelling and Dynamic Analysis of Gearless Variable-Speed Permanent Magnet Synchronous Generator Based Wind Energy Conversion System,” *Int. Conf. Renew. Energies Power Qual.*, vol. 1, no. 10, pp. 1597–1602, 2012.

[47] G. Azevedo, “Modeling of a Variable Speed Wind Turbine with a Permanent Magnet Synchronous Generator,” *IEEE Int. Symp. Ind. Electron. (ISIE 2009)*, pp. 734–739, 2009.

[48] P. Badoni and S. B. Prakash, “Modeling and Simulation of 2 MW PMSG Wind Energy Conversion Systems,” *IOSR J. Electr. Electron. Eng.*, vol. 9, no. 4, pp. 53–58, 2014.

[49] A. Abdulslam, B. Mohammad, M. Ismail, and Y. Ismail, “A simple hybrid 3-level buck-boost DC-DC converter with efficient PWM regulation scheme,” in *Proceedings of the IEEE International Conference on Electronics, Circuits, and Systems*, vol. 2016–March, 2016, pp. 368–371.

[50] M. . Camara, B. Dakyo, and H. Gualous, “Permanent Magnet Synchronous Generators for Offshore wind energy system linked to Grid -Modeling and Control Strategies,” *Int. Power Electron. Motion Control Conf. Expo.*, pp. 165–169, 2014.

[51] “Park Transform.” [Online]. Available: https://www.mathworks.com/help/physmod/sps/ref/parktransform.html.

[52] S. S. Kulkarni and A. G. Thosar, “Mathematical Modeling and Simulation of Permanent Magnet Synchronous Machine,” in *International Journal of Electronics and Electrical Engineering*, 2013, vol. 1, no. 2, pp. 66–71.

[53] S. Li, T. A. Haskew, R. P. Swatloski, and W. Gathings, “Optimal and Direct-Current Vector Control of Direct-Driven PMSG Wind Turbines,” *IEEE Trans. Power Electron.*, vol. 27, no. 5, pp. 2325–2337, 2012.

[54] L. G. González, E. Figueres, G. Garcerá, and O. Carranza, “Modelling and Control in Wind Energy Conversion Systems (WECS),” *13th Eur. Conf. Power Electron. Appl. Barcelona, Spain*, 2009.

[55] P. C. Krause, O. Wasynczuk, and S. D. Sudhoff, *Analysis of Electric Machinery and Drive System*, Second Edi. Wiley, 2002.

[56] U. Ramanjaneya Reddy and B. L. Narasimharaju, “Single-Stage Electrolytic Capacitor less Non-Inverting Buck-Boost PFC Based AC-DC Ripple Free LED Driver,” *IET Power Electron.*, vol. 10, no. 1, pp. 38–46, 2017.

[57] S. Dong, Y. Wang, and H. Li, “Coordinated Control for Active and Reactive Power of PMSG-based Wind Turbine to Enhance the LVRT Capability,” *15th Int. Conf. Electr. Mach. Syst.*, pp. 1–4, 2012.

[58] R. Mittal, “Low Voltage Ride-Through (LVRT) of Grid Interfaced Wind Driven PMSG,” *J. Eng. Appl. Sci.*, no. October, 2015.

[59] K. Qu, J. Zhao, and Y. Xing, “A LVRT Control Strategy Based on DC-link Voltage Limit for PMSG Wind Generation System,” *IEEE 7th Int. Power Electron. Motion Control Confrences- ECCE*, pp. 1169–1172, 2012.

ملخص البحث

تعد طاقة الرياح من مصادرالطاقة النظيفة والمهمة اقتصادياً. تتطورت موارد الطاقة المتجددة تتطوراً سريعاً و بالأخص المعتمدة منها علي طاقة الرياح للمنافسة مع غيرها من مصادر الطاقة وذلك نتيجة النقص المتزايد في موارد الطاقة التقليدية المعتمدة على الوقود الاحفوري. بسبب الطبيعة المتغيرة للرياح ، تم تطوير العديد من استراتيجيات التحكم لاستخراج الطاقة القصوى من توربينات الرياح.

تتناول هذة الرسالة دراسة لنظام تحويل طاقة الرياح متغيرة السرعة، عن طريق أستخدام محول التضاد. يعتمد النظام المقترح علي المولد المتزامن ذو المغنطة الدائمة مفتوح الملفات والذي بات يجذب الإنتباه في السنوات القليلة الماضية. كما قدمت الرسالة محول التيار المتردد الي الثابت باستخدام محول الكترونى خافض- رافع للجهد والذي تم التحكم فية بأسلوب التوصيل المتقطع حيث يجعل التيار المصدر ذو تموج جيبي ويتمتع بمعامل قدرة أحادي القيمة. في البداية، تمت دراسة ومحاكاه محول التيار المتردد الي الثابت أحادي الطور، ثم تم تقديم التصميم الخاص بالمحول ثلاثي الطور واللذى تم استخدامه فى محول التضاد.

يتكون نظام تحويل طاقة الرياح المقترح من مولد متزامن ذو مغنطة دائمة ثلاثي الطور، متصلاً بثلاثة محولات متوازية يتكون كل منهم من محول التيار المتردد الي الثابت أحادي الطور. تنقسم تقنية التحكم المتبعة الي جزئين أساسيين، الجزء الأول وهو الخاص بالمحول خافض- رافع الجهد المتصل وذلك لتتبع نقطة القدرة القصوي عن طريق تقنيين سرعة المولد عند القيمة المثلى والتحكم بتيار المولد. أما أستراتيجية التحكم الأخري وهي الخاصة بعاكس الجهد الالكترونى المتصل بالشبكة للتحكم بنقل القدرة الي الشبكة. يتصل المحول الخاص بجانب المولد و المحول الخاص بجانب الشبكة عن طريق مكثف.

علاوة علي ذلك، تم تطبيق إستراتيجية مواكبة الجهد المنخفض للمنظومة المقترحة لضمان موثوقية وإستدامة النظام المقترح لتحويل طاقة الرياح. تعد أستراتيجية مواكبة الجهد المنخفض من أهم متطلبات اكواد الشبكات الكهربية لنظم تحويل طاقة الرياح والتى تحدد حالة مزرعة الرياح اثناء حدوث خلل بالشبكه الكهربيه. تمت محاكاه النظام المقترح ودراسة أداؤة تحت ظروف تشغيل مختلفة باستخدام برنامج PSCAD/EMTDC.

الأكاديمية العربية للعلوم والتكنولوجيا والنقل البحرى

كلية الهندسة و التكنولوجيا

قسم الهندسة الكهربائية و التحكم

نظام تحويل طاقة الرياح بأستخدام مولد متزامن ذو مغنطة دائمة مفتوح الملفات مع محول التيار المتردد الي الثابت عن طريق خافض-رافع للجهد

رسالة مقدمة من

مهندسة: نهي مجدي عبدالخالق عطية

للحصول علي درجة الماجيستير
في
الهندسة الكهربية و التحكم

تحت إشراف

الاستاذ الدكتور: مصطفي إبراهيم مرعي

قسم هندسة القوي والآلات الكهربية
جامعة عين شمس

الدكتور: إبراهيم عبدالله عبد السلام

قسم الهندسة الكهربائية والتحكم
الأكاديمية العربية للعلوم والتكنولوجيا والنقل البحري

القاهرة

2019

الأكاديمية العربية للعلوم والتكنولوجيا والنقل البحرى

كلية الهندسة و التكنولوجيا

قسم الهندسة الكهربائية و التحكم

نظام تحويل طاقة الرياح باستخدام مولد متزامن ذو مغنطة دائمة مفتوح الملفات مع محول التيار المتردد الي الثابت عن طريق خافض-رافع للجهد

رسالة مقدمة من

مهندسة: نهي مجدي عبدالخالق عطية

للحصول علي درجة الماجيستير
في
الهندسة الكهربية و التحكم

تحت إشراف

الاستاذ الدكتور: مصطفي إبراهيم مرعي

قسم هندسة القوي والآلات الكهربية
جامعة عين شمس

الدكتور: إبراهيم عبدالله عبد السلام

قسم الهندسة الكهربائية والتحكم
الأكاديمية العربية للعلوم والتكنولوجيا والنقل البحري

القاهرة

2019